MOLECULAR DYNAMICS SIMULATIONS OF ALKALI HALIDE CLUSTERS

By

Timothé Croteau

B. Sc. (Chemistry) McGill, 2001

A THESIS SUBMITTED IN PARTIAL FULFILLMENT OF

THE REQUIREMENTS FOR THE DEGREE OF

MASTER OF SCIENCE

in

THE FACULTY OF GRADUATE STUDIES

(Department of Chemistry)

We accept this thesis as conforming

to the required standard

THE UNIVERSITY OF BRITISH COLUMBIA

September 2004

Library Authorization

In presenting this thesis in partial fulfillment of the requirements for an advanced degree at the University of British Columbia, I agree that the Library shall make it freely available for reference and study. I further agree that permission for extensive copying of this thesis for scholarly purposes may be granted by the head of my department or by his or her representatives. It is understood that copying or publication of this thesis for financial gain shall not be allowed without my written permission.

TIMOTHÉ CROTEAU
Name of Author *(please print)*

09/09/2004
Date (dd/mm/yyyy)

Title of Thesis: Molecular Dynamics Simulations of Alkali Halide Clusters.

Degree: Msc. Year: 2004

Department of Chemistry
The University of British Columbia
Vancouver, BC Canada

Abstract

An investigation of the melting, freezing and structure of pure LiCl, KCl and mixed LiCl-KCl clusters is presented. The results of molecular dynamics simulations of unconstrained neutral clusters with 6, 8, 10, ..., 32, 64, 216, 512, and 1000 ions have been carried out using the Born-Mayer-Huggins potential based on a rigid ion (non-polarizable) approximation. Initial molecular dynamics studies of phase transitions in clusters of alkali halides have shown some very interesting characteristics, especially in the case of large size asymmetry where the ionic radii ratio, $r_+/r_- \leq 0.5$. A comparison of the structures of KCl and LiCl clusters coupled with the calculation of the mean square displacement and distribution of the ions about the center of mass allows us to discuss the relevance of size asymmetry effects on the melting temperature, and on the stability of different isomeric structures. The main conclusion regarding pure LiCl clusters is that the behaviour of the LiCl pairs is greatly influenced by their strong dipolar character. This is shown by the clear competition between ring-like and cubic structures. For LiCl clusters, the strong dipolar character favours the formation of less ordered expanded ring structures explaining the absence of a sharp melting transition. At the solid-liquid transition, the energies associated with the liquid and solid structures are very similar possibly explaining the early melting of LiCl when compared with the other alkali halide salts. The study of binary mixtures shows that the structures are insensitive to LiCl concentration for a broad range of composition. The cubic character of KCl clusters tends to dominate over the strong dipolar character of LiCl clusters which creates a separation or segregation of the species. Specifically, ion segregation effects give rise to a cubic portion in the structure of clusters with a LiCl mole fraction as high as 0.333, whereas ring geometries

only start to appear when the KCl mole fraction is reduced to 0.093. Moreover, it is only when the mole fraction of either KCl or LiCl has reached 0.95 that the properties of the pure cluster are observed.

Table of Contents

List of Figures

List of Tables

List of Symbols

Symbol	Description
a	The acceleration vector
A	Dynamical variable
α_i	The polarizability of ion i
β	The Pauling exclusion coefficient
C_{ij}	The coefficients for the dipole-induced dipole interactions
D_{ij}	The coefficients for the dipole-induced quadrupole interactions
D	The self diffusion constant
ϵ	Energy strength parameter
f	Force vector
H	The Hamiltonian
k_B	The Boltzmann constant
K	The kinetic energy of the system
$L(t)$	The Liouville operator
m	Mass
μ	Dipole moment
n_t	The number of different time origins
N	The number of particles
Ω	Octopole moment
p	Generalized particle momenta
P	The pressure of a system of particles

ϕ	Interaction potential
q	Point charge
$\mathbf{q}$	Generalized particle coordinates
$\mathbf{r}_i$	Position vector
r_{ij}	Interionic distance
r_+, r_-	Cation and anion radii
R_e	Equilibrium bond length
ρ	Hardness parameter
σ	Length parameter
δt	Small time increment (time step)
t	Time
T	Temperature
Θ	Quadrupole moment
$u_{ij}(r_{ij})$	The potential energy between two particles separated by a distance r_{ij}
U	The total potential energy of the system
$\mathbf{v}$	Velocity vector
V	The volume of a system of particles
x	Mole fraction

Acknowledgement

I wish to thank my supervisor, Dr. Gren Patey, for his guidance and excellent intellectual, physical, and social support, who made this experience a truly beneficial one. I also want to thank the members of my lab for their help. Finally, I want to thank my relatives and friends who encouraged me all along these past two years.

Chapter 1

Introduction

In the 20th century, a lot of effort was concentrated towards obtaining an understanding of clusters of atoms, molecules and ions due to their important role in nature. In the early stages, most of the work concentrated on the investigation of simple homogeneous systems made of neutral spherically symmetric particles such as hard spheres, or rare gases assumed to interact through a Lennard-Jones potential [1–4]. Over the years, ever increasing computational power coupled with a better understanding of homogeneous systems led to the development of more sophisticated theoretical models to study more complex systems. Nowadays, there exist a large range of different clusters under investigation (alkali halides [5–8], rare gases doped with a large organic molecule [9,10], nanoclusters [11,12], dipolar materials [13]). The topics studied have also increased considerably, including phase behaviour (freezing, melting), interfacial phenomena, crystal growth, and ionic crystal films. In spite of this impressive list, there is still much to be learned about the variability of cluster behaviour.

Our primary interest in the study of alkali halide clusters comes from the fact that they are amenable to both theory and experiment. They are in fact one of the simplest and one of the best model systems to investigate the interactions between charged particles. Much of the work done on these systems to describe their interactions is attributed to the efforts of Born, Mayer, Huggins [14], Pauling [15], and Fumi and Tosi [16]. The creation of a realistic pairwise additive potential stands as a culmination of many decades of development. Meanwhile, experimentalists have made great advances in refining their

techniques to investigate the mechanism of cluster ion formation for the alkali halides. Modern techniques now include particle sputtering [17,18], vapour condensation in an inert-gas atmosphere [19,20], and laser vapourization of a crystal surface [21,22]. Cluster ion formation with these techniques is greatly influenced by the conditions under which it is performed. The initial gas temperature and the cooling rate are important factors determining the size distribution of clusters. Under certain conditions, such as an expanding molecular jet, it is possible to obtain very rapid and efficient evaporative cooling which limits the cluster growth to small clusters. In this case, the final cluster size distribution is mainly determined by the high-temperature cluster stability. For sodium chloride cluster ions $Na(NaCl)_n^+$, clusters at n = 13, 22, 37, 62, and 87 are the most abundant and have a cubic structure resembling a fragment of crystal lattice [21].

Probably the most important and interesting aspect of this study is to relate structural changes of alkali halide clusters occurring during heating or cooling to their phase behaviour. To this end, molecular dynamics simulations provide an ideal method to study the dynamical and structural behaviour of these systems. The choice of clusters instead of bulk systems comes directly from their different intrinsic characteristics. Firstly, results obtained by Luo, Landman and Jortner [7] have shown that NaCl clusters of different sizes have different phase behaviour. Small clusters present simple isomerization behaviour whereas large clusters present freezing-melting behaviour. Also, the results obtained so far for many different alkali halides show that they all have different apparent temperatures for both melting and freezing transitions. This phenomena where the apparent melting temperature, T_{am}, is higher than the apparent freezing temperature, T_{af}, is known as hysteresis. As opposed to the bulk, clusters do not necessarily present phase coexistence. Actually, there is practically no phase coexistence when the number of ions is less than 1000 [23]. Recently, *ab initio* studies made on several small alkali halide clusters have shown a clear separation in the behaviour of the clusters at an

interionic size ratio $r_+/r_- = 0.5$ [24]. Above this value small clusters always form cubic structures, whereas when the size asymmetry becomes large, $r_+/r_- \leq 0.5$, the clusters tend to form ring-like structures. This is the case for most of the Li halide clusters including LiF and LiCl.

These ring structures were also encountered in a study of the ground state configurations of model molecular dipolar clusters using Monte Carlo simulations [25]. In this study, Clarke and Patey showed that small dipolar hard sphere clusters with a small quadrupole moment and small polarizability form ring structures. On the other hand, a larger quadrupole moment or polarizability causes the rings to collapse into asymmetric structures or to break into chains (see Fig. 1.1 and Fig. 1.2). This means that ring formation is more likely to be observed when the higher order interactions in the multipole expansion, such as quadrupole and octopole interactions vanish. This way, the dipolar interactions are dominant and the molecules are greatly influenced by their dipolar character. Also, if the higher order moments are sufficiently large the ring structures become unstable and the cluster dipole moment can be quite large. Based on the above results, we calculated the dipole (μ), and higher order moments up to n=7 of a LiCl and KCl pair using the equilibrium bond lengths for our model to determine the relative importance of their dipolar character (see Table 1.1). In these calculations, the origin (i.e. the point about which the multipole expansion is made) was chosen to be at the mid-point along the equilibrium bond length. Using this origin, instead of the commonly used center of mass origin, has the effect of producing, for linear molecules such as LiCl and KCl, null multipole moments for even orders of n and simplifies the analysis. For linear molecules, the odd multipole moments are given by [26]

$$\mu = \sum_i q_i \mathbf{r}_i, \tag{1.0.1}$$

$$\Omega = \sum_i q_i \mathbf{r}_i \mathbf{r}_i \mathbf{r}_i, \tag{1.0.2}$$

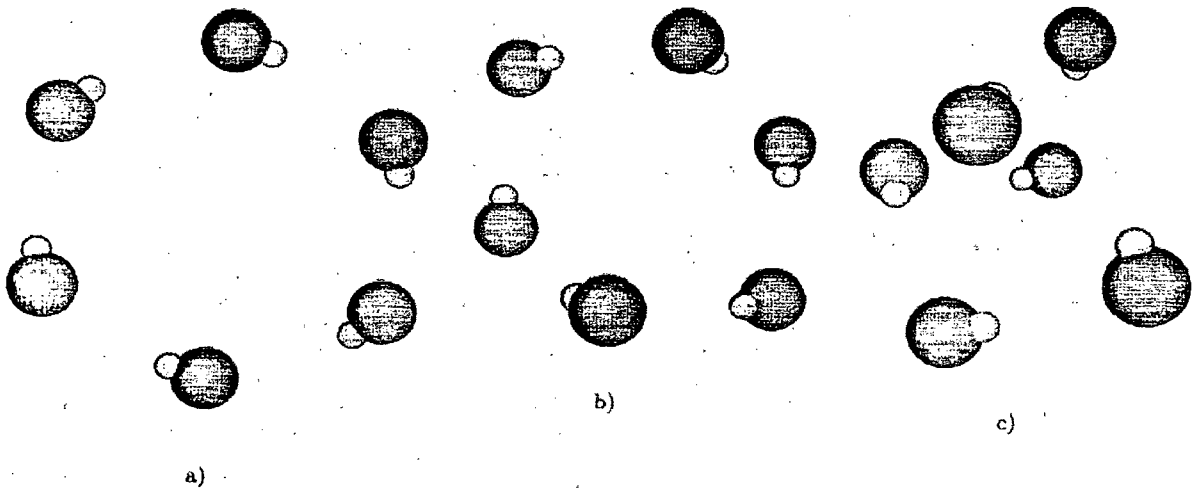

Figure 1.1: Ground state configurations for dipolar/quadrupolar hard sphere clusters of six particles. The quadrupole moments are (a) Q^*=0.25, (b) Q^*=0.5, and (c) Q^*=0.75. The cluster with Q^*=0.25 is nearly planar, but for Q^*=0.5 and Q^*=0.75 the clusters are three dimensional. The reduced quadrupole moment, Q^*, is defined by $Q^{*2}=Q^2/(\epsilon\sigma^5)$. Each cluster is drawn in perspective so that near particles appear to have a larger diameter than far particles. The data was obtained by Clarke and Patey [25].

and so on. Here q is the charge, μ the dipole moment, and Ω the octopole moment.

From Table 1.1, it is observed that the KCl pair has a greater dipole moment than the LiCl pair by a factor of about 1.42 which, at first sight, would imply that it has a more important dipolar character than LiCl. However, KCl also has larger higher order moments compared to LiCl. And the difference in magnitude increases with n (see Table 1.1). Therefore, it is this larger contribution from the higher order moments in KCl that is responsible for breaking the alignment of the KCl pairs and favors cubic structures. Therefore, from this purely electrostatic argument, it is postulated that the behaviour of the LiCl pairs is greatly influenced by their dipolar character since they have a smaller contribution from their higher order moments compared to KCl. This hypothesis was confirmed by the use of Molecular Dynamic simulations for some LiCl clusters.

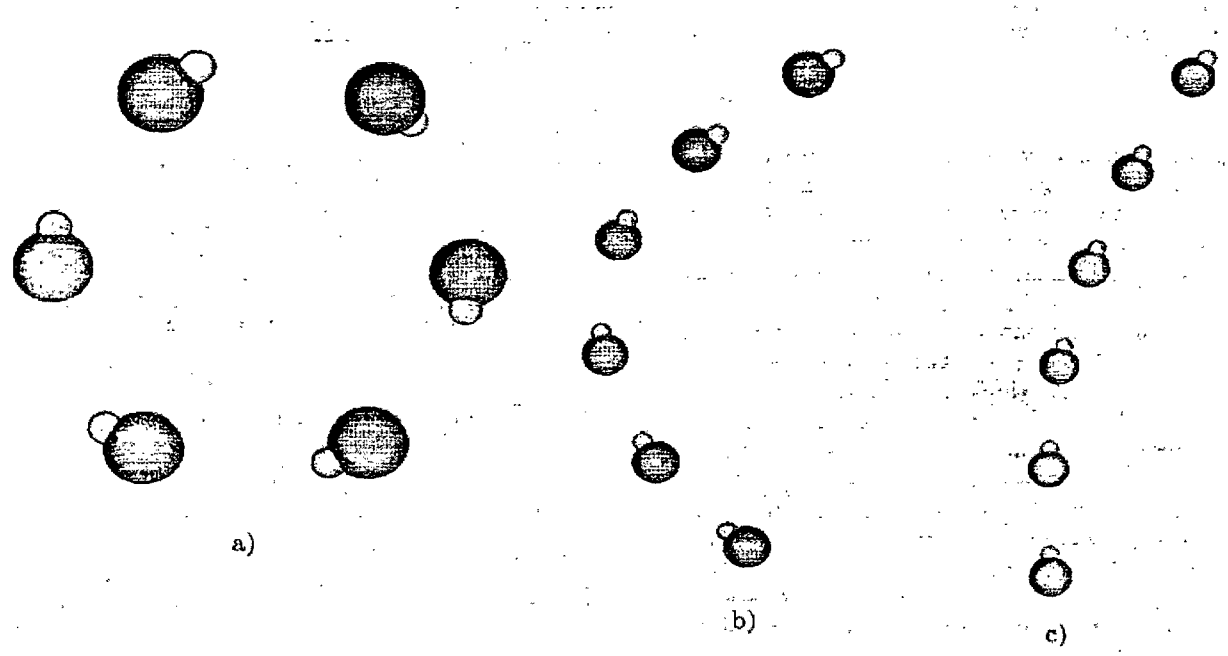

Figure 1.2: Monte Carlo results for clusters of six polarizable dipolar hard sphere particles. Ground state configurations for (a) α^*=0.04, (b) α^*=0.06, and (c) α^*=0.08. For α^*=0.04 the ground state configuration is a ring. For α^*=0.06 the ground state configuration is a bent chain. As the polarizability increases from 0.06 to 0.08 [parts (b) and (c)] the chain straightens. The reduced polarizability, α^*, is defined by $\alpha^*=\alpha/\sigma^3$. Each cluster is drawn in perspective so that near particles appear to have a larger diameter than far particles. The data was obtained by Clarke and Patey [25].

Table 1.1: Calculated dipole (μ) ,octopole (Ω), and higher order moments (given in SI units) and equilibrium bond lengths for our model (R_e) for KCl and LiCl.

Molecule	μ (x$10^{-29}Cm$)	Ω (x$10^{-49}Cm^3$)	$n=5$ (x$10^{-69}Cm^5$)	$n=7$ (x$10^{-89}Cm^7$)	R_e (x$10^{-10}m$)
$^7Li^{35}Cl$	2·932	2·455	2·055	1·720	1·83
$^{39}K^{35}Cl$	4·149	6·959	11·67	19·57	2·59

The study of binary mixtures is also of interest as they are technologically very important systems. Due to their lower melting-freezing temperature binary and ternary mixtures have been used in many industrial processes such as preparation of metals [27], nuclear reactors [28], and batteries [29]. It is thus relevant to investigate their properties on a molecular dynamics basis. Towards this end, recent simulations of the liquid-vapour interface of size asymmetric molten binary mixtures [30], such as LiCl-KCl, have shown the importance of clustering effects due to the fact that the Li^+ and K^+ ions have different coordination numbers in the bulk, respectively 4 and 6. This geometrical difference creates a constrained environment where each species tries to attain its most favourable state. This can lead to the segregation of one of the species towards the surface as was the case in the study described in Ref. [30].

The remainder of this thesis is divided into three chapters. Chapter 2 presents an overview of the statistical mechanical and computer simulation methods used to study the behaviour of some small salt clusters over a wide temperature range, including the melting and freezing transitions. The structural and dynamical information obtained from molecular dynamics simulations for LiCl, KCl, and KCl-LiCl binary mixtures is presented and discussed in Chapter 3. Finally, a summary of the conclusions reached is given in Chapter 4.

Chapter 2

Simulation Methodology

The field of modern theoretical and computational chemistry offers a wide variety of tools and methods to study numerous physical processes. One of the most commonly used techniques, which has received an enormous increase in both power and versatility is computer simulation. With the creation of modern super-computers capable of simulating systems with a large number of particles (e.g. cracking or fracture problems with millions of atoms [31]) problems that seemed intractable not long ago are now possible to probe.

Over the years, the number of simulation techniques has expanded. There exist now many specialized techniques for particular problems, including quantum mechanical or classical simulations. Two such techniques were developed to study physical and biological processes, namely, molecular dynamics (MD), and Monte Carlo (MC) methods [32]. Both of these complementary methods can simulate a system at equilibrium. Molecular dynamics simulations provide the means to solve the equations of motion of the particles to produce the trajectories of a system. With molecular dynamics simulations, one can study equilibrium properties as time averages over the history of the system. MD simulations have provided detailed information on the study of complex, dynamical processes that occur in physical and biological systems.

On the other hand, Monte Carlo simulations are a statistical means of obtaining the equilibrium state of a system. The essential characteristic of Monte Carlo is the use of random sampling techniques to arrive at a solution of the physical problem. In computational chemistry this method most commonly involves a system of "Monte Carlo moves".

These moves correspond to perturbations usually applied on the particle's position or orientation. If the move leads to a lower energy state it is automatically accepted. If not, it is accepted with a probability given by a Boltzmann factor. The repetition of this sampling process will finally produce a collection of configurations representing an equilibrium ensemble for specific state conditions. It can then be used to calculate some of the physical properties of the system as ensemble averages. Monte Carlo is now used routinely in many diverse fields, from the simulation of complex physical phenomena such as radiation transport in the earth's atmosphere and the simulation of subnuclear processes in high energy physics experiments. The great advantage of this technique comes from the versatility of the permutation algorithm. In addition to the exchange of energy (canonical ensemble), it is a simple matter to allow the exchange of particles to sample from the grand canonical ensemble.

Conversely, the strength of the molecular dynamics method comes directly from the integration of the equations of motion leading to the time evolution of the trajectories. As was the case for Monte Carlo simulations, different ensembles can be produced by controlling thermodynamic quantities such as temperature and pressure. The microcanonical ensemble (constant NVE) is often used and is formed by integrating the unconstrained Newtonian equations of motion. Another very useful ensemble is the canonical ensemble (NVT) where the temperature is controlled by a thermostat. By definition, this uses non-newtonian equations of motion as they include modifications in their description to control the temperature. In this case care must be taken to avoid non-physical effects while removing energy from the system. As we are interested in the dynamical and structural behaviour of clusters at the melting-freezing transition, the MD simulation was chosen to pursue the current study.

2.1 Statistical Mechanics

The connection between microscopic behaviour and macroscopic properties is made via statistical mechanics. It provides the rigorous mathematical expressions that relate macroscopic properties to the distribution and motion of the atoms and molecules of an N-body system. Consider a classical system of N spherical particles which can be fully described by a set of $3N$ generalized coordinates $\mathbf{q} = (q_1, q_2, ..., q_N)$ and a set of $3N$ generalized momenta $\mathbf{p} = (p_1, p_2, ..., p_N)$ that evolve in time [33]. The propagation in time of these generalized parameters will generate a trajectory determined by the initial state point and the equations of motion. The fundamental microscopic equation governing the behaviour of the distribution function in classical statistical mechanics is the Liouville equation,

$$\frac{df(t)}{dt} = -iL(t)f(t), \tag{2.1.1}$$

where $f(t)$ is the distribution function and the Liouville operator is defined as

$$iL(t)A = \{A, H(t)\}, \text{classical}, \tag{2.1.2}$$

where $\{..., ...\}$ denotes Poisson brackets. The classical Hamiltonian, H, which describes the system is given by

$$H(p, q) = K(p) + U(q), \tag{2.1.3}$$

where $K(p)$ is the kinetic energy and $U(q)$ is the total potential energy. The motion of the spherical particles in this system are governed by $6N$ first-order differential equations:

$$\dot{q} = \frac{\partial H}{\partial p} \tag{2.1.4}$$

$$\dot{p} = -\frac{\partial H}{\partial q}. \tag{2.1.5}$$

Given that the $3N$ generalized coordinates and the $3N$ generalized momenta are known at a particular instant, the subsequent dynamics of the system is uniquely determined by the known laws of molecular dynamics. It is useful to represent the state of the

entire system as a point in $6N$ dimensional phase space. Of course this point traces out a path as the system evolves in time. However, since the system is isolated, its energy is constant (conserved) and so the path is restricted to lie on a fixed energy surface. Now, we are usually interested not in the detailed time evolution of the state but rather in its macroscopic properties in thermodynamic equilibrium. Let $A(q(t), p(t))$ be some physical quantity written as a function of the state of the system. The time average of A is given by

$$\bar{A} = \lim_{t\to\infty} \frac{1}{t} \int_0^t A(q(t), p(t))dt. \tag{2.1.6}$$

Of course, in a simulation or even in an experiment it is impossible to go to infinite times. Instead, one actually measures the time average of the quantity of interest over a period that is very long compared to the mean molecular collision time. It is also important to make sure that the system has reached equilibrium before performing any averages by looking at a conserved quantity. The conserved quantity can either be the total energy (NVE), the kinetic energy (NVT), or the pressure (NPT) depending on the type of simulations performed. If the conserved quantity has no propensity to drift over a sufficiently long period of time, then the system has most likely attained equilibrium. Once equilibrium has been reached the average values of the desired quantities can be obtained using Eq. (2.1.6).

One of the great advantages of MD simulations has to do with the large number of physical quantities that can be calculated. With the coordinates and momenta of all particles known at all times quantities that are impossible to get from experiment are now easily computed using MD. For instance, in the present study we are interested in the behaviour of small clusters at the boundary between the solid and liquid phases. By using the time evolution of the particles we are able to obtain some fascinating information about structural arrangements, mobilities, and distribution of ions.

The signature of the melting-freezing transition is best observed by calculation of the caloric curve that is obtained by plotting the temperature as a function of the total energy of the cluster. At the level of the equipartition theorem the temperature is proportional to the average kinetic energy. A system of N particles, with a stationary center of mass and no rotational kinetic energy has a temperature,

$$T = \frac{2 < E_{kinetic} >}{(3N-6)k_B}, \tag{2.1.7}$$

where the angular brackets denote an average over the whole trajectory, k_B is the Boltzmann constant, and $E_{kinetic}$ is the total kinetic energy.

In the present study, the caloric curve was obtained either by slowly heating the cluster, by scaling the momenta until evaporation occurred, or by quickly heating the cluster to a temperature well into the liquid state and then slowly removing energy until the system reached the desired temperature.

Small clusters often present significant physical differences with respect to the bulk phase. In general, finite size systems do not have sharp transitions. Instead, a retardation in the response of the system around the melting-freezing transition causes a temperature difference upon heating and cooling. This phenomena is known as hysteresis and renders ambiguous the determination of the melting-freezing temperature as it does not have a sharp well-defined value. Though, an approximate value of the melting temperature can be obtained by averaging the higher melting and lower freezing temperatures. Also, while the structural possibilities are limited for the bulk material, the number of different isomers that may exist for clusters is usually large, and the energy differences between isomers are often small. Recent *ab initio* studies on small clusters [24,34] have shown that large size asymmetric clusters, such as LiF and LiCl which have an interionic distance at equilibrium, $r_+/r_- \leq 0.5$, tend to form ring-like structures. In these cases, the determination of the state of a cluster during heating may become difficult due to

the presence of many possible low-lying isomers. A definition of "liquid-like" for a cluster based on the motions of the ions was given by Rose and Berry: "To be liquid-like, the facile interwell motions of the cluster must generate particle interchanges so that the cluster explores its permutational isomers on a time scale approaching that of the vibrations. In the solid-like state particles do not permute among different sites and exhibit negligible diffusion" [35].

An informative way of determining if a system is fluid is through the mean square displacement (MSD),

$$< r^2(t) > = \frac{1}{N n_t} \sum_{j=1}^{n_t} \sum_{i=1}^{N} [r_i(t_{0j} + t) - r_i(t_{0j})]^2, \tag{2.1.8}$$

where n_t is the number of different time origins and t_{0j} is the time step at time origin j. The slope of the MSD curve as a function of time for bulk matter is proportional to the diffusion constant, D

$$D = \frac{1}{6} \frac{d}{dt} < r^2(t) > . \tag{2.1.9}$$

For bulk systems, if the system is in the solid state the slope of the MSD curve will quickly increase to finally reach a plateau. On the other hand, if the system is in the liquid state the slope of the MSD curve will increase linearly with temperature. Similarly, it is possible to obtain relevant information about the state of a cluster by taking into account finite size effects which can modify the shape of the liquid and solid curves. For example, the slope of the liquid MSD curve must have a plateau at long times as the ions cannot go beyond a certain distance for a fixed temperature. The determination of the liquid state itself can sometimes be ambiguous. As will be seen later, structural rearrangements ocurring during heating may increase the motion of the ions producing a nonzero value of D while still being solid. This would give rise to an irregular pattern in the MSD curve. Also, note that at long times the accuracy of the MSD curve decreases due to lesser sampling. Therefore, to avoid confusion the long time part of the MSD

curves was eliminated. Otherwise, one could think that the observed sudden change in the slope of the MSD curve corresponds to different mobility modes whereas these are due to poor sampling. Nevertheless, the transitions are usually accompanied by a large change in the value of D making them easy to determine. In the case of the binary KCl-LiCl mixtures, with large differences in the physical properties of pure KCl and LiCl such as bulk melting point, it may be possible to observe phase separation as one species freezes before the other as indicated by the slopes of their respective MSD curves.

Another useful means of obtaining equilibrium structural information is through the distribution of ions relative to the center of mass. This function was calculated for every species by binning the distance relative to the center of mass of every ion to an array of size 25. Each one of the 25 divisions of the array corresponds to a distance interval covering one unit length ranging from 0 to 24 $\mathring{A}$ (e.g. 0-1, 1-2, ..., 24-∞). Every time an ion was found at a specific distance interval a value of one was added to the corresponding memory location. This process was repeated 5000 times at every temperature to get a good statistical average.

A change in the distribution pattern of a solid structure for pure clusters can indicate the occurance of a structural rearrangement. On the other hand, the large size asymmetry in binary systems has led to the calculation of different bulk coordination numbers for KCl and LiCl [30]. This different behaviour may be observed during the freezing process with the segregation of one species. If the other species is left at the surface or in any other concentrated region the distribution pattern of the solid structure would immediately reflect this, leaving a near null concentration at all other locations.

2.2 Intermolecular Potentials

For a system of N interacting particles with positions r^N, the general form of the total configurational energy, U, is given by an expansion series [36]

$$U(r^N) = \sum_{ij} u(r_i, r_j) + \sum_{ijk} u(r_i, r_j, r_k) + ..., \tag{2.2.1}$$

where the first term represents a pairwise sum, the second term a triplet sum, and so forth. Although it is desirable to include as many terms as possible to represent correctly the interactions among the particles, the computational cost quickly increases and limits the capacity. Moreover, since relatively little is known about the higher order terms most simulation studies are restricted to pairwise additive terms only. Instead, most models are devised in such a way as to implicitly include the higher order contributions. In a previous study [15] this was achieved by assuming a typical solid density and adjusting the parameters of the pairwise additive potentials so as to reproduce thermodynamic data obtained from experiment.

The model produced for the pair potential can take many different forms depending on the system under investigation. For most simple systems such as nonpolar spherical particles, the existing models are well characterized by a repulsive and an attractive term. In our case, the interactions among positively and negatively charged ions coupled with dispersion forces, as temporary induced dipoles are formed upon the approach of two adjacent ions, are the main sources of the attraction. The repulsive contribution of the overlap of electron orbitals as the ions are brought into close proximity results in a steeply repulsive barrier at short separations. This short-range repulsive interaction accounting for the Pauli exclusion principle is most widely represented by either an exponential or a r^{-12} dependence term characteristic of Lennard-Jones particles.

In the case of interest a non-polarizable rigid ion model (RIM) is most commonly used. For charged spherical particles the main contribution to the attractive interactions

is known to be of Coulombic nature and has an r^{-1} dependence. Linus Pauling was the first to give a successful form to the repulsive interaction in crystals through a $1/r^n$ dependence, where n was usually given the value 9 [15], followed by Born, Mayer and Huggins [14] who developed an equivalent exponential term. Many refinements of this potential concerning the inclusion of induced dipolar interactions as well as polarizability in the case of strongly asymmetric salts have been proposed. One such possible variation is the inclusion of induced multipole interactions, i.e., dipole-induced dipole and dipole-induced quadrupole interactions [37].

These corrections were included in the present study to yield the Born-Mayer-Huggins (BMH) form [29,38,37], with parameters due to Tosi and Fumi [16]

$$U = \sum_{ij} u_{ij}(r_{ij}) = \sum_{ij} \left\{ \frac{q_i q_j}{r_{ij}} + \beta_{ij} b \exp\left\{ \frac{[(\sigma_i + \sigma_j) - r_{ij}]}{\rho_{ij}} \right\} + C_{ij} r_{ij}^{-6} + D_{ij} r_{ij}^{-8} \right\}, \quad (2.2.2)$$

where q_i is the ionic charge of ion i, taken as $+e$ and $-e$ for the cation and anion respectively, e is the elementary charge, r_{ij} is the distance between ions i and j, β_{ij} is the Pauling exclusion coefficient, b is a positive constant [15], ρ is the hardness parameter, and C_{ij} and D_{ij} are respectively the coefficients for the dipole-induced dipole and dipole-induced quadrupole interactions. The parameter values are given in Table 2.1 for the two alkali halides considered here. The cross-interaction between ions having different energy parameters (β_{ij}, C_{ij} and D_{ij}) and length parameters (ionic radii), denoted respectively as ϵ and σ, were determined using the Lorentz-Berthelot rules, $\sigma_{12} = (\sigma_{11} + \sigma_{22})/2$ and $\epsilon_{12} = \sqrt{\epsilon_{11}\epsilon_{22}}$. A plot of a typical BMH potential is shown in Fig. 2.1.

The BMH potential has had much success in reproducing bulk thermodynamic properties. For example, it reproduced, using the above Tosi-Fumi parameters, the solid and liquid molar volumes and molar enthalpies at the normal melting temperatures within a few percent of the reported experimental values [16]. Moreover, as discussed below in Section 3.1, this potential agrees well with *ab initio* calculations made on small alkali halide

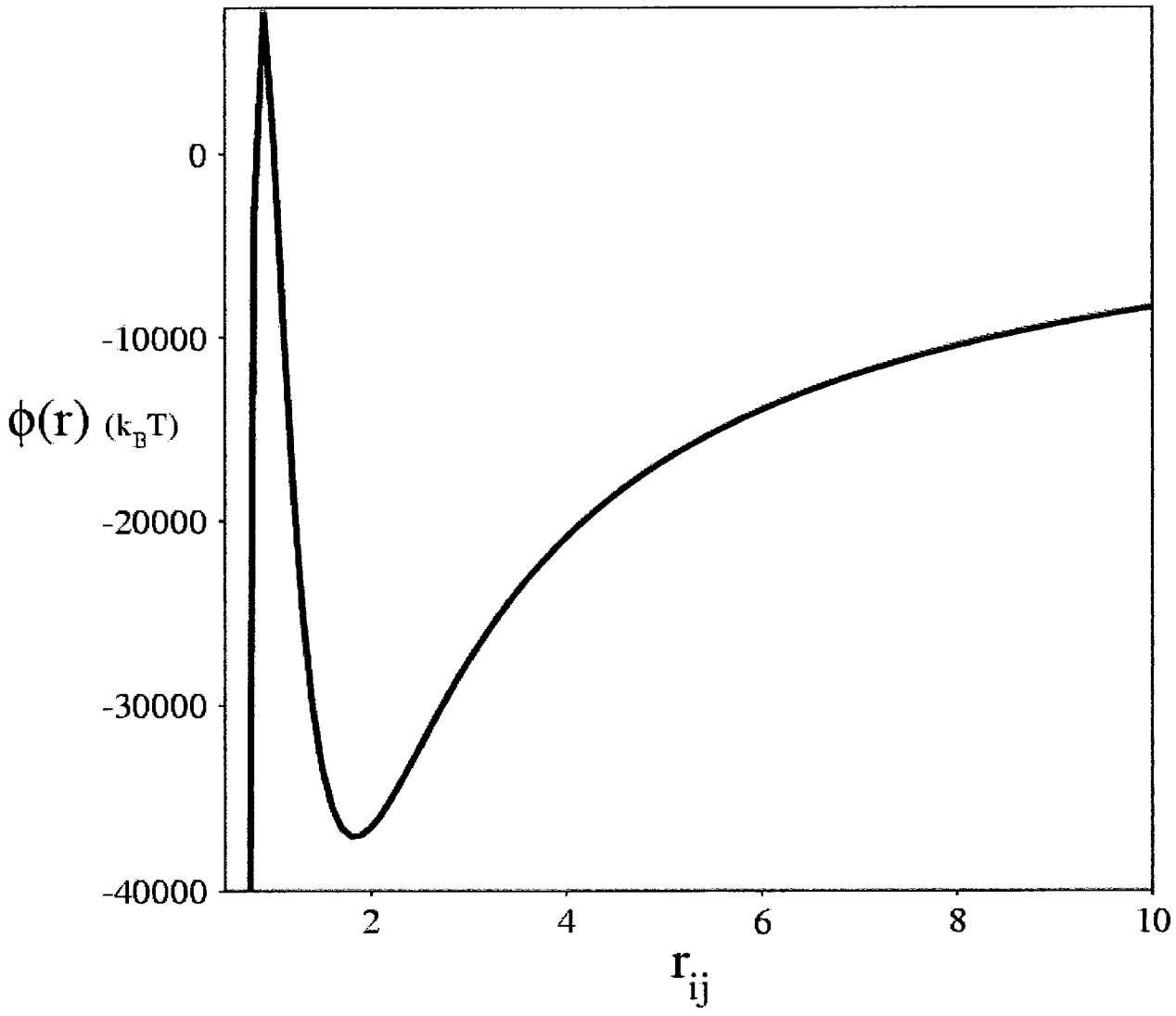

Figure 2.1: Form of the standard BMH potential for one LiCl pair. r_{ij} is in $\mathring{A}$.

Table 2.1: Tosi-Fumi parameters [16] for the BMH potential. The cation and anion are denoted by + and −, respectively, and b = 0.338x10^{-19} J.

Salt	Species pair	$(\sigma_i + \sigma_j)$ ($\AA$)	$\beta_{ij}b$ (10^{-19} J)	ρ_{ij}^{-1} ($\AA^{-1}$)	$-C_{ij}$ (10^{-19} $J\AA^6$)	$-D_{ij}$ (10^{-19} $J\AA^8$)
LiCl	++	1.632	0.676	2.92	0.073	0.03
LiCl	+−	2.401	0.465	2.92	2.0	2.4
LiCl	−−	3.170	0.253	2.92	111.0	223.0
KCl	++	2.926	0.423	2.97	24.3	24.0
KCl	+−	3.048	0.338	2.97	48.0	73.0
KCl	−−	3.170	0.253	2.97	124.5	250.0

clusters. Based on the above statements it was judged unnecessary to include corrections regarding the polarizability of the ions and it was decided to use the Born-Mayer-Huggins potential for the entire study.

2.3 Molecular Dynamics

As mentioned previously, the present study solely relies on the molecular dynamics simulation method. To simulate real systems at a finite temperature, we need to find ways to reproduce the motions of the particles. This is achieved by the numerical integration of the equations of motion for a system of N particles interacting via a pairwise additive potential. Let $u_{ij}(r_{ij})$ be the potential between two neighboring particles i and j, separated by a distance r_{ij}. The total force acting on particle i is given as a sum over all the interactions with the neighbouring particles [36]

$$\mathrm{f}_i = \sum_{j \neq i} -\frac{du_{ij}(r_{ij})}{dr_{ij}}. \tag{2.3.1}$$

The classical equations of motion describing a system of N particles are represented by a collection of ordinary differential equations. There are several different algorithms to choose between for integrating the equations of motion. An important point to consider

is the accuracy of the algorithm to produce the same trajectories forward and backward in time (time-reversible), so that the initial state can always be traced back, with the largest time step possible. Because the force calculation is the most time consuming part, we want to maximize the time interval between each such calculation. Another important criterion is the conservation of energy. Thus, a good algorithm is one which does not tend to have drift in the energy for long times for the largest time step possible. Once we have chosen a suitable algorithm, a trajectory can be produced by updating the positions and velocities at time t to time $t + \delta t$ through the integration of the equations of motion.

In molecular dynamics, the most commonly used time integration algorithm is probably the so-called Verlet algorithm [39]. The basic idea is to write two Taylor series expansions for the positions, one forward and one backward in time

$$\mathsf{r}_i(t + \delta t) = \mathsf{r}_i(t) + \delta t \dot{\mathsf{r}}_i(t) + \frac{1}{2}\delta t^2 \ddot{\mathsf{r}}_i(t) + \ldots, \tag{2.3.2}$$

$$\mathsf{r}_i(t - \delta t) = \mathsf{r}_i(t) - \delta t \dot{\mathsf{r}}_i(t) + \frac{1}{2}\delta t^2 \ddot{\mathsf{r}}_i(t) - \ldots. \tag{2.3.3}$$

Adding the two expressions gives

$$\mathsf{r}_i(t + \delta t) = 2\mathsf{r}_i(t) - \mathsf{r}_i(t - \delta t) + \delta t^2 \ddot{\mathsf{r}}_i + \ldots. \tag{2.3.4}$$

This is the basic form of the Verlet algorithm. Since we are integrating Newton's equations, the acceleration is obtained from its relationship with the force

$$\mathsf{f}_i = m_i \mathsf{a}_i. \tag{2.3.5}$$

A problem with this version of the Verlet algorithm is that velocities are not directly generated. While they are not needed for the time evolution, knowledge of them is sometimes necessary. Moreover, they are required to compute the kinetic energy K, whose evaluation is necessary to test the conservation of the total energy $E = K + U$.

This is one of the most important tests to verify that a MD simulation is proceeding correctly.

To overcome this difficulty, other variants of the Verlet algorithm have been implemented. One of the best modifications is the velocity-Verlet method [32,40], which computes the particle position and velocity at time $t + \delta t$ as follows:

$$\mathsf{r}_i(t + \delta t) = \mathsf{r}_i(t) + \delta t \mathsf{v}_i(t) + \frac{1}{2}\delta t^2 \frac{\mathsf{f}}{m}. \tag{2.3.6}$$

$$\mathsf{v}_i(t + \delta t) = \mathsf{v}_i(t) + \frac{[\mathsf{f}(t) + \mathsf{f}(t + \delta t)]}{2m}\delta t. \tag{2.3.7}$$

Given the initial conditions one can compute the updated positions and velocities simply by applying Eq. (2.3.6) and Eq. (2.3.7) successively to produce a phase space trajectory.

The fifth-order Gear predictor-corrector is another slightly more complex method. It calculates the particle's position based on a Taylor series expansion

$$\mathsf{r}_i(t + \delta t) = \mathsf{r}_i(t) + \delta t \dot{\mathsf{r}}_i(t) + \frac{1}{2}\delta t^2 \ddot{\mathsf{r}}_i + \ldots, \tag{2.3.8}$$

and also predicts dynamical information about the acceleration of the particle in the same fashion

$$\mathsf{a}_i(t + \delta t) = \mathsf{a}_i(t) + \delta t \dot{\mathsf{a}}_i(t) + \frac{1}{2}\delta t^2 \ddot{\mathsf{a}}_i + \ldots, \tag{2.3.9}$$

where the dots indicate differentiation with respect to t.

Both algorithms presented here usually satisfy very well the conservation criterion discussed above. As to which one should be more efficient and give better results depends on the situation. In fact, both algorithms are likely to give satisfactory efficiency. The choice of algorithm was based on the fact that other similar studies involving alkali halide clusters used for the most part the simpler velocity-Verlet method. Also, remember that we were able to reproduce *ab initio* calculations for some small alkali halide clusters (see Section 3.1).

Chapter 3

Results and Discussion

Molecular dynamics calculations were performed on neutral alkali halide clusters of different sizes ranging from 6 to 1000 ions, as summarized in Table 3.1. As shown in Table 3.1, most of the attention was put towards the study of pure LiCl and binary KCl-LiCl clusters over a wide range of sizes and concentrations. The case of pure KCl has been the object of several previous studies and serves more as a comparison tool, allowing us to distinguish the different features of systems with larger size asymmetry. Small neutral clusters ranging from 6 to 20 ions were used to test the accuracy of both the simulation method and BMH potential by comparing them with the minimum energy configurations obtained by Aguado *et al.* in their study using the *ab initio* perturbed ion (PI) method [24]. This method is a quantum chemical approach to the solution of the Schrödinger equation in ionic materials and involves the theory of electron separability. For all clusters listed in Table 3.1, a caloric curve was produced by heating and/or cooling the system. In both cases, the clusters were started on a fcc lattice that was not necessarily the ground state. Upon heating, structural changes would often occur before melting. These changes were either driven by entropy to produce higher energy configurations or simply by rearrangement to a lower energy structure for those systems that were not initially in the ground state. Similarly, cooling the system from an equilibrium molten state produced some of the most stable solid structures for a given cluster and unraveled some interesting structural details. These results were checked by heating and cooling again to see if the clusters found a different low energy configuration. These frozen structures

Table 3.1: A summary of the systems simulated.

systems	Number of pairs	x_{LiCl}	x_{KCl}
Pure KCl	$3-10, 32, 108$	0.0	1.0
Pure LiCl	$3-16, 32, 108, 256, 500$	1.0	0.0
		0.969, 0.688, 0.563	0.969, 0.812, 0.687
$(\mathrm{LiCl})_n - (\mathrm{KCl})_{32-n}$	64	0.500, 0.406, 0.313	0.594, 0.500, 0.437
		0.188, 0.031	0.313, 0.031
		0.954, 0.907, 0.852	0.954, 0.907, 0.852
$(\mathrm{LiCl})_n - (\mathrm{KCl})_{108-n}$	108	0.75, 0.667, 0.491	0.741, 0.667, 0.574
		0.426, 0.333, 0.259	0.509, 0.333, 0.25
		0.148, 0.093, 0.046	0.148, 0.093, 0.046

were particularly of interest in the case of LiCl clusters as stable non-cubic structures were always produced, many of which led to a lower energy configuration. In the case of the larger symmetric 2n x 2n x 2n magic number alkali halide clusters, in addition to the caloric curve the distribution of ions relative to the center of mass and mean square displacement (MSD) of every ionic species were obtained at each temperature.

3.1 Small neutral alkali halide clusters

Figure 3.1 shows the lowest energy structures obtained by Aguado *et al.* [24] for small KCl and LiF clusters. In this study, the authors proposed a simple explanation for the different structural trends observed: an interionic distance at equilibrium $r_+/r_- \leq 0.5$ favours the formation of hexagonal ring isomers, whereas when $r_+/r_- \geq 0.5$, cubic structures are obtained. In this respect, LiCl falls in the same category as LiF as they both have an interionic distance at equilibrium, $r_+/r_- \leq 0.5$. This allows us to make a direct comparison of the structures obtained for some small KCl and LiCl clusters with their *ab initio* calculations.

Table 3.2 presents some of the low energy structures obtained and their associated

Table 3.2: A summary of the low energy structures obtained for small clusters, and their associated energies. Note that some of the energies, marked by a *, were extrapolated to zero temperature. The energies are in eV/ion.

Number of pairs	Structure	KCl	LiCl
3	hexagonal ring	-3.078	-3.935
4	cube	-3.206	-3.952
4	ring	-3.081*	-4.008*
5	chair	-3.211*	–
5	ring	-3.142*	-4.037
6	cubic	-3.278	–
6	double ring	-3.261*	-4.068*
7	*ab initio* ground state	-3.272*	–
8	cubic	-3.348	–
8	double ring	–	-4.093*
9	cubic	-3.349	–
9	triple ring	-3.343	-4.125
16	hexagonal rings	–	-4.182
16	cubic	–	-4.171*

energies. The results obtained are in clear agreement with the proposed trend as LiCl clusters prefer to form ring-like structures and KCl clusters prefer to form cubic structures. Moreover, the low energy structures obtained are in excellent agreement with the above *ab initio* calculations, at least for the ground state and low-lying isomers. For example, the low energy cubic structures made of 5, 6, 7, 8, and 9 pairs (Fig. 3.1) were never obtained for LiCl. Instead, only ring structures were formed. Still, these results match with the low energy minimization as all the low energy ring structures formed agree with the calculated ground states (Fig. 3.1). Conversely, small KCl clusters always preferably formed the low energy cubic structures with the possibility to rearrange to a higher energy ring structure.

As a first example of the different behaviour, Fig. 3.2 and Fig. 3.3 show the caloric curves for both $(KCl)_4$ and $(LiCl)_4$, starting the simulation in the fcc structure. In

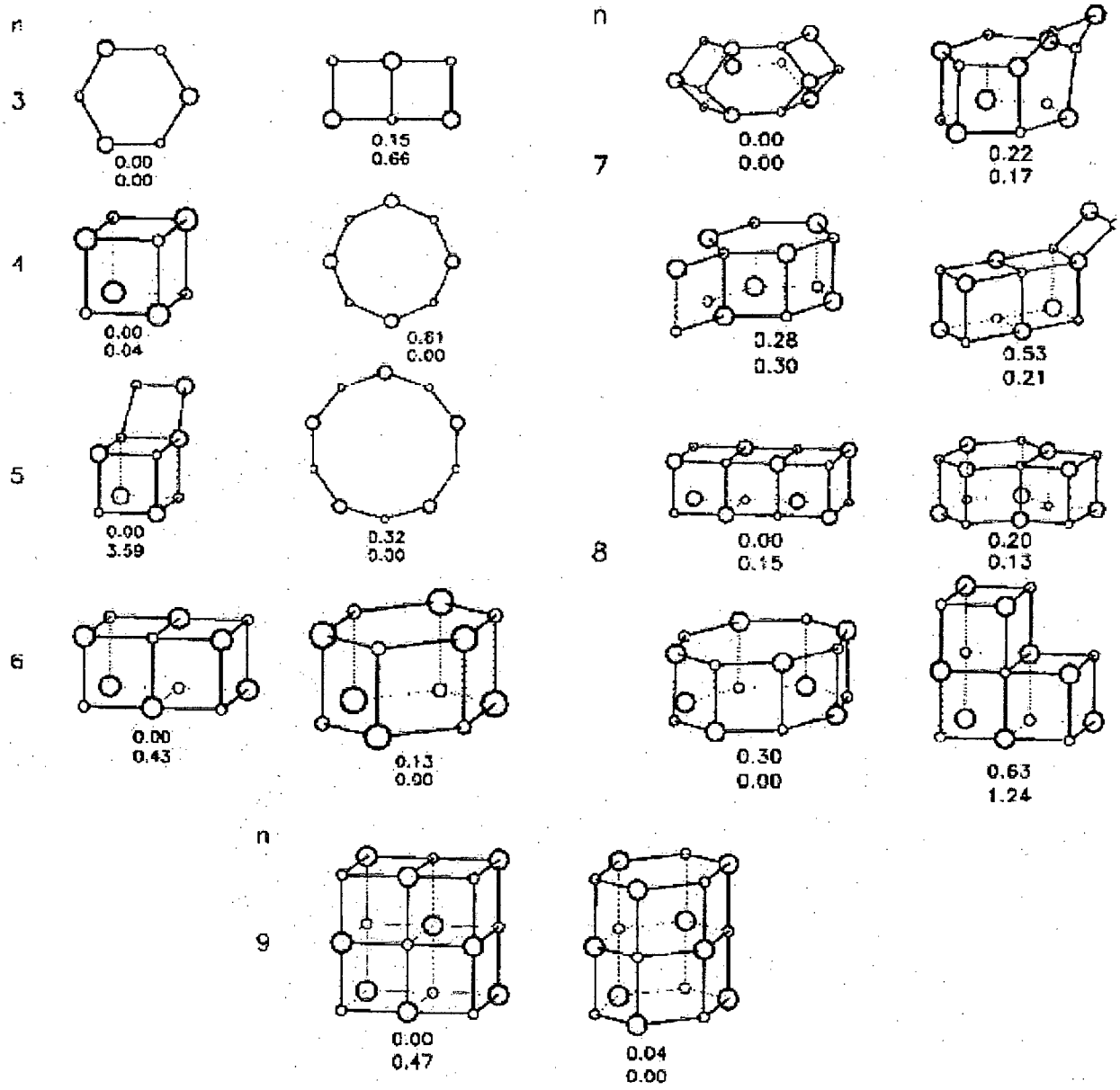

Figure 3.1: Lowest-energy structures and low-lying isomers of $(LiF)_n$ and $(KCl)_n$ clusters. The energy difference (in eV) with respect to the most stable structure is given below the corresponding isomers. The first value corresponds to KCl and the underlying value corresponds to LiF. Stability decreases from left to right for $(KCl)_n$ clusters. Data obtained by Aguado *et al.* [24]

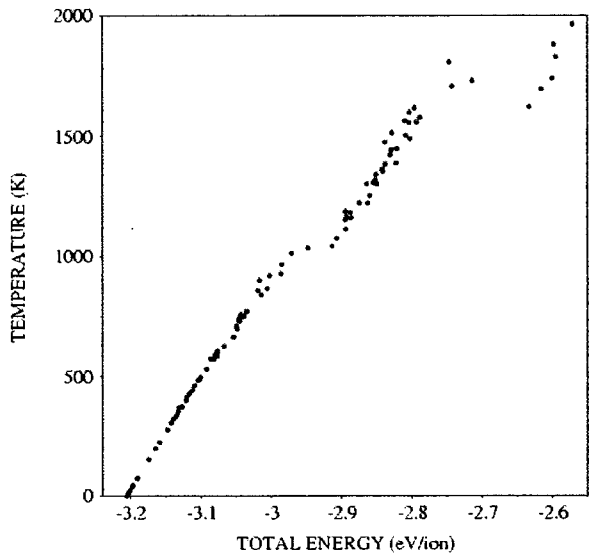

Figure 3.2: Caloric curve obtained by heating $(KCl)_4$. The transition occurring at -2.95eV/ion corresponds to melting. The large change in energy occurring at -2.75eV/ion corresponds to evaporation.

agreement with Fig. 3.1, these simulations show us that the ground state of $(KCl)_4$ is the fcc structure as it only undergoes rearrangement to a higher energy 8-membered ring upon melting (at -2.95eV/ion), whereas $(LiCl)_4$ transforms to the low energy ring structure before it melts (at -3.88eV/ion). For $(LiCl)_4$, a disruption at $\simeq$-3.83eV/ion indicates that melting has occurred from a ring structure.

From the above structural correspondance with *ab initio* calculations we were highly confident with the simulation method and went on to unexplored territory. The structural study of $(LiCl)_{16}$ was our first new piece of information in the investigation of the interesting behaviour associated with LiCl. By starting the system on a fcc lattice and following a caloric curve (see Fig. 3.4) the ions quickly rearranged themselves to a lower energy state immmediately after the first temperature increment to finally form the expanded non-symmetric ring structure (Fig. 3.5) at around 190K. In cooling the system

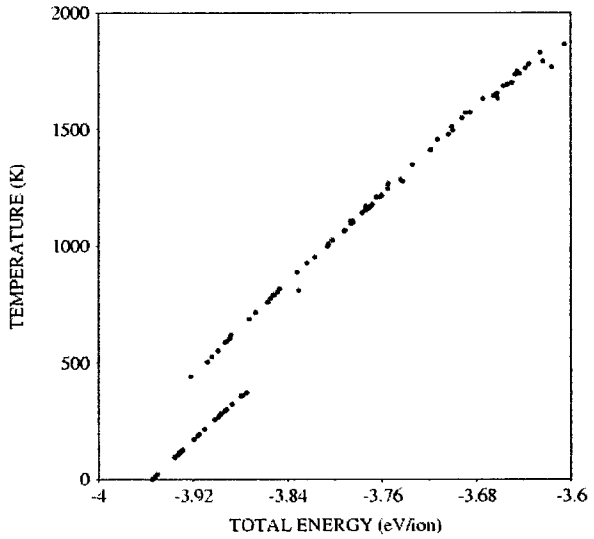

Figure 3.3: Caloric curve obtained by heating $(LiCl)_4$. The change in energy occurring at -3.87eV/ion corresponds to the rearrangement of the cubic structure to the lower energy ring structure. The small disruption at -3.83eV/ion corresponds to melting. Evaporation occurs at -3.63eV/ion.

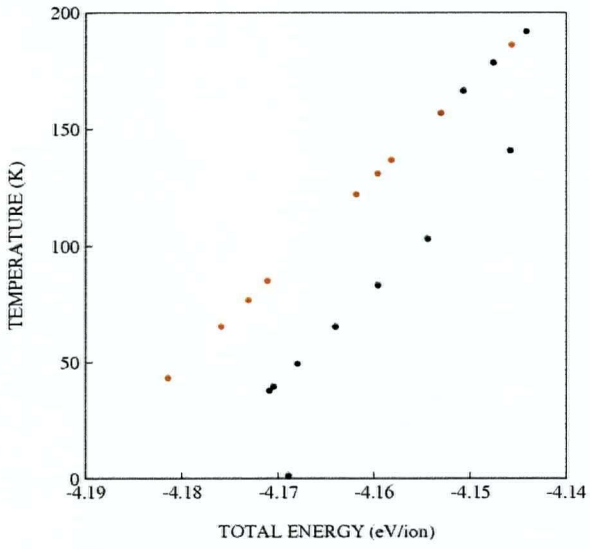

Figure 3.4: Caloric curve for $(LiCl)_{16}$. The curve starts at -4.169eV/ion. The system quickly rearranges to a slightly lower energy configuration (-4.171eV/ion) and the heating (black dots) continues up to -4.145eV/ion where the final rearrangement occurs. After that, further heating did not produce any other rearrangement to a lower energy structure and the cluster was cooled (red dots) into its low energy structure at -4.181eV/ion.

down, the extrapolated energy of that configuration was found to be -4.182 eV/ion which is lower than the rock salt structure, $\simeq$ -4.17 eV/ion. Thus, the minimum energy configuration for $(LiCl_{16})$ is not cubic. Looking carefully at the last image in Fig. 3.5, which shows a view of the surface through the cluster structure, it is possible to observe that the basic building block of this structure actually is the hexagonal ring.

As opposed to Aguado *et al*, we already mentioned in Chapter 1 that our explanation for the tendency of LiCl clusters to form ring geometries goes beyond the above classification using the interionic distance at equilibrium r_+/r_-. Instead, the formation of these very particular ring geometries are caused by the strong dipolar character of LiCl. The formation of these ring structures will be encountered at every step in the analysis of the behaviour of the LiCl clusters.

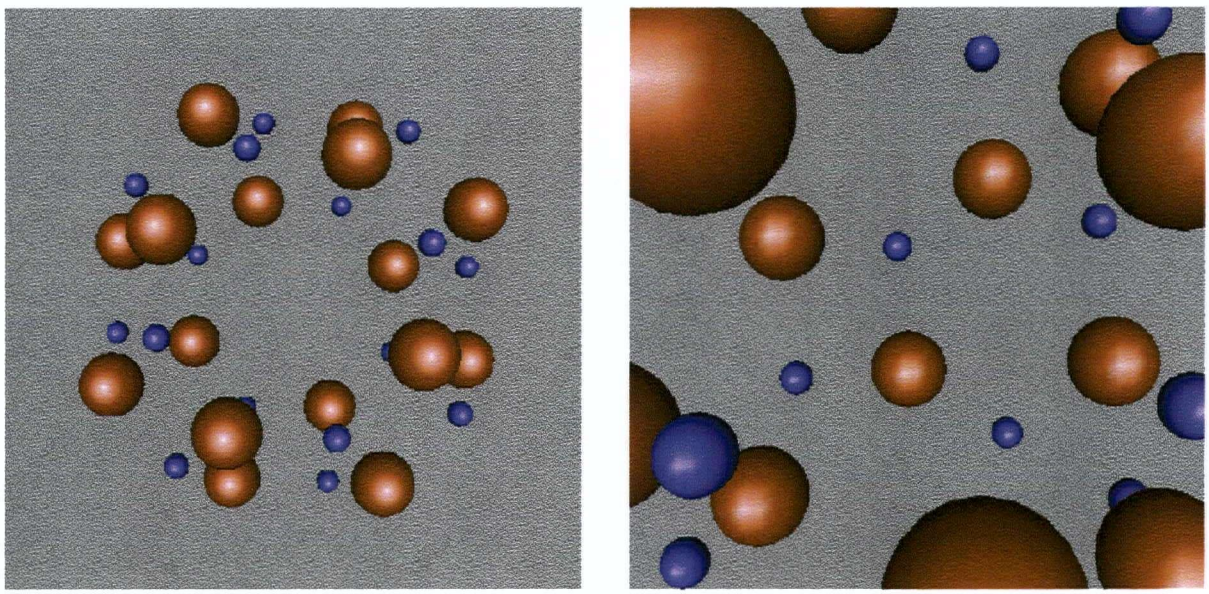

Figure 3.5: Snapshots of $(LiCl)_{16}$. The purple and red colours correspond respectively to the $Li^+$and Cl^- ions. To the left is the low energy solid structure and to the right is a view of its ring-like surface.

3.2 $(KCl)_{32}$ and $(KCl)_{108}$

There have been a number of KCl studies already reported in the literature [35,41]. So, our intention here is mainly to use this system as an example to show some of the intrinsic features of small clusters, and to compare with the LiCl case which has a strong dipolar character. As all the larger magic number KCl clusters, the smallest being $(KCl)_4$, behave in essentially the same way, it was judged sufficient to use only the second and third smallest magic number clusters. Figure 3.6 shows the caloric curves for both these clusters, namely, $(KCl)_{32}$ and $(KCl)_{108}$. Both clusters exhibit a solid-like low temperature phase and a liquid-like high temperature phase. They also transform between these two phases in a very small energy interval. As soon as the energy is high enough, the cluster passes out of its equilibrium solid-like state and melts rapidly from a still cubic structure (Fig. 3.7). Note from Fig. 3.6 the large change in temperature associated with the melting transition. This is supported by Rodrigues and Silva Fernandes [23] who concluded in their study of large clusters that there is no phase coexistence at all for clusters with less than 200 ions. Furthermore, these clusters exhibit pronounced hysteresis. It is not yet clear if this is simply due to size effects, or if it is a combination of some artefacts of the MD simulation regarding the fast heating and cooling rates. It is also worth mentioning the sharpness in energy of the melting transition as shown in Fig. 3.6 and from the MSD curve, Fig. 3.8. The bottom curve has nearly a null slope whereas the slope of the top curve clearly indicates that the cluster has now became fluid. The distribution of ions along the heating curve doesn't change much until melting, which also shows that the cluster melts from a cubic structure (see Fig. 3.7 and Fig. 3.9). Another feature of small KCl clusters is that the melting temperature approaches the experimental value as the size of the cluster increases, as reported by Rodrigues and Silva Fernandes [23] (see also Fig. 3.6).

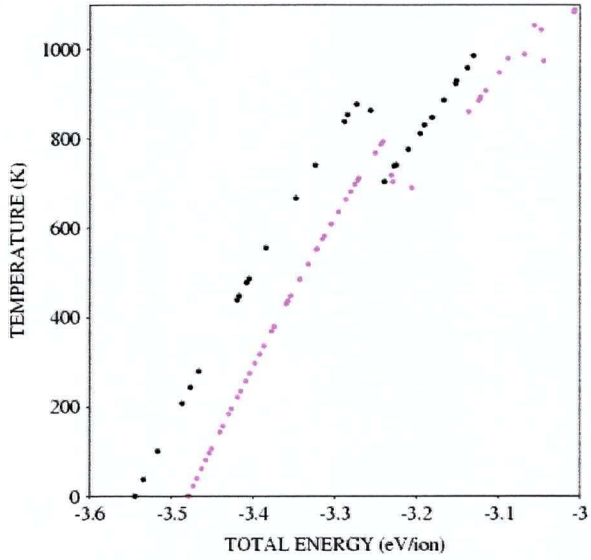

Figure 3.6: Caloric curves obtained by heating both $(KCl)_{32}$ (pink) and $(KCl)_{108}$ (black). Melting occurs at $\simeq$ -3.25eV/ion in both cases. Evaporation occurs above -3.1eV/ion.

3.3 Dipolar effect on the larger magic number LiCl clusters

The two previous sections served as a prelude to the most interesting part of this work. By studying the case of small clusters we learned that the strong dipolar character of LiCl tends to create ring structures. On the other hand, the straightforward case of KCl was very informative, and will be useful to make comparisons with the larger LiCl clusters. Noting this, let's see what kind of structural behaviour the strong dipolar character of LiCl creates for larger clusters.

In order to observe the behaviour of LiCl we obtained caloric curves for the next four larger magic number clusters, $(LiCl)_{32}$, $(LiCl)_{108}$, $(LiCl)_{256}$, and $(LiCl)_{500}$. In all experiments, the system was started in the fcc structure and remained there until a sudden rearrangement occurred above 120K (see Fig. 3.10 and Fig. 3.11). In order to convince ourselves that this low temperature change was reproducible and was not due

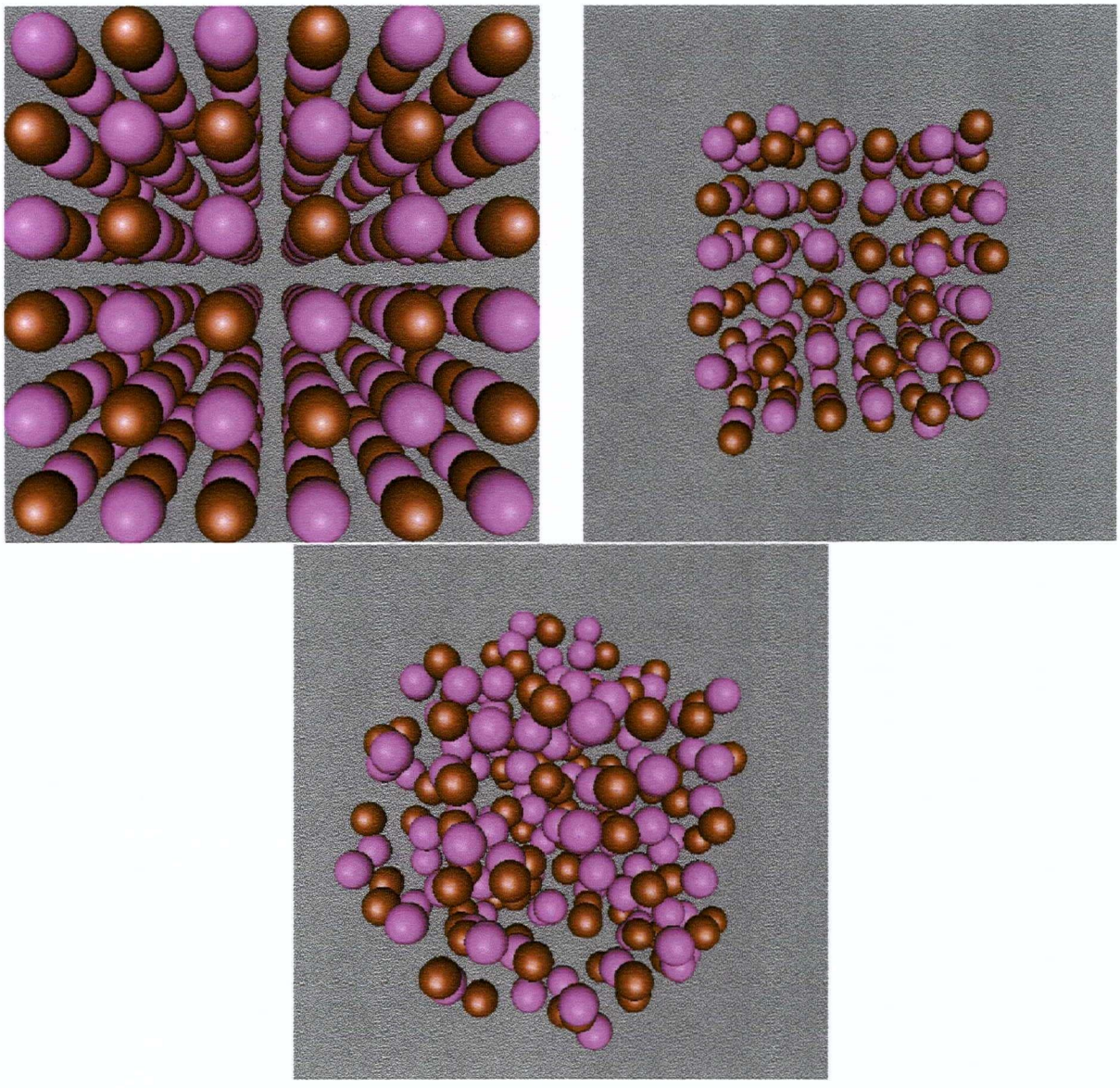

Figure 3.7: Snapshots for $(KCl)_{108}$. Shown are the fcc structure (top left), the cubic structure before melting at -3.27eV/ion (top right), and the molten structure at -3.24eV/ion. The pink and red colours correspond to the K^+ and Cl^- ions.

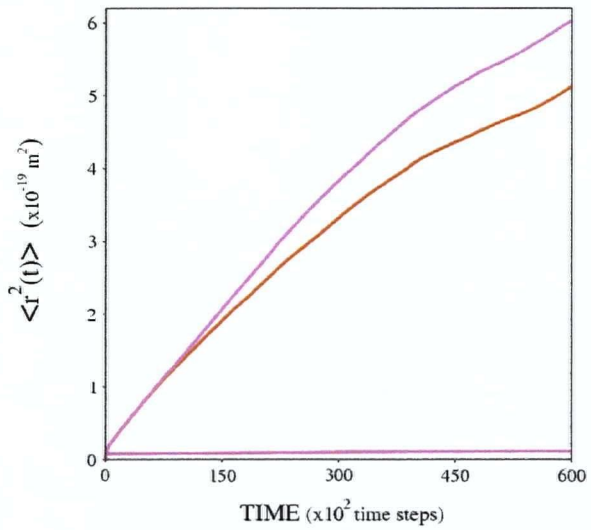

Figure 3.8: MSD curves at melting for $(KCl)_{108}$. The top and bottom curves, corresponding to the molten and frozen state, were calculated at -3.24eV/ion and -3.27eV/ion. The pink and red colours correspond to the K^+ and Cl^- ions.

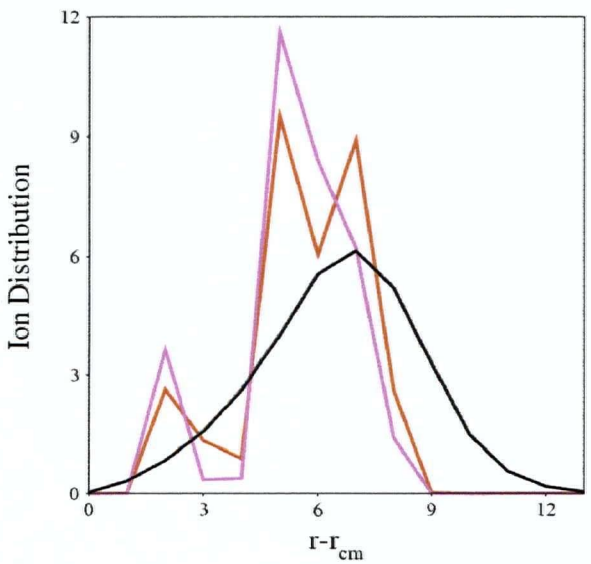

Figure 3.9: Ion distributions relative to the center of mass for $(KCl)_{108}$. The red, pink, and black lines correspond respectively to the cubic structure at -3.55eV/ion and just before melting at -3.27eV/ion, and the liquid structure immediately after melting at -3.24eV/ion.

Table 3.3: A summary of the low energy structures obtained for large LiCl clusters and their associated energies. Note that some of the energies, marked by a *, were extrapolated to zero temperature. The energies are in eV/ion.

Cluster size	fcc structure	ring structure
$(LiCl)_{32}$	-4.226	-4.236
$(LiCl)_{108}$	-4.285	-4.271
$(LiCl)_{256}$	-4.311	-4.30*
$(LiCl)_{500}$	-4.325	-4.31*

to premature melting of the clusters we made, for $(LiCl)_{108}$, a series of runs starting at different temperatures, thereby producing different trajectories, all crossing the threshold temperature (see Fig. 3.12). In all runs a change occurred at the same temperature going from the fcc structure to a less ordered expanded ring structure (see Fig. 3.16 for an example). Figure 3.13 presents an example of the MSD curves obtained for those structures before and after the transformation occurred showing by their null slopes that it is due to a structural change, and not due to a premature melting of the cluster. Further heating of the clusters induced a continuous series of rearrangements until melting finally occurred. The energies of the fcc structure and most stable isomer obtained for all four clusters are summarized in Table 3.3. In one case only did this transformation to a stable ring structure lead to a lower energy state, as seen from the end of the cooling part of the caloric curve for $(LiCl)_{32}$ (Fig. 3.10). In all other cases a higher energy state was produced, meaning that different processes are driving these changes (see Table 3.3). For $(LiCl)_{32}$ it is simply due to rearrangement to a more favorable state with lower energy. In the other cases, entropy driven transitions to the higher energy states occurred.

The melting transitions, as seen from the caloric curves in Fig. 3.10 and Fig. 3.11, were not as sharp in energy as for $(KCl)_{32}$ and $(KCl)_{108}$ (Fig. 3.6) and melting seems to be more of a continuous process. However, the freezing transition is sharper for $(LiCl)_{108}$ (see Fig. 3.10). Accordingly, the MSD curves (Fig. 3.14) for the melting transition occurring at

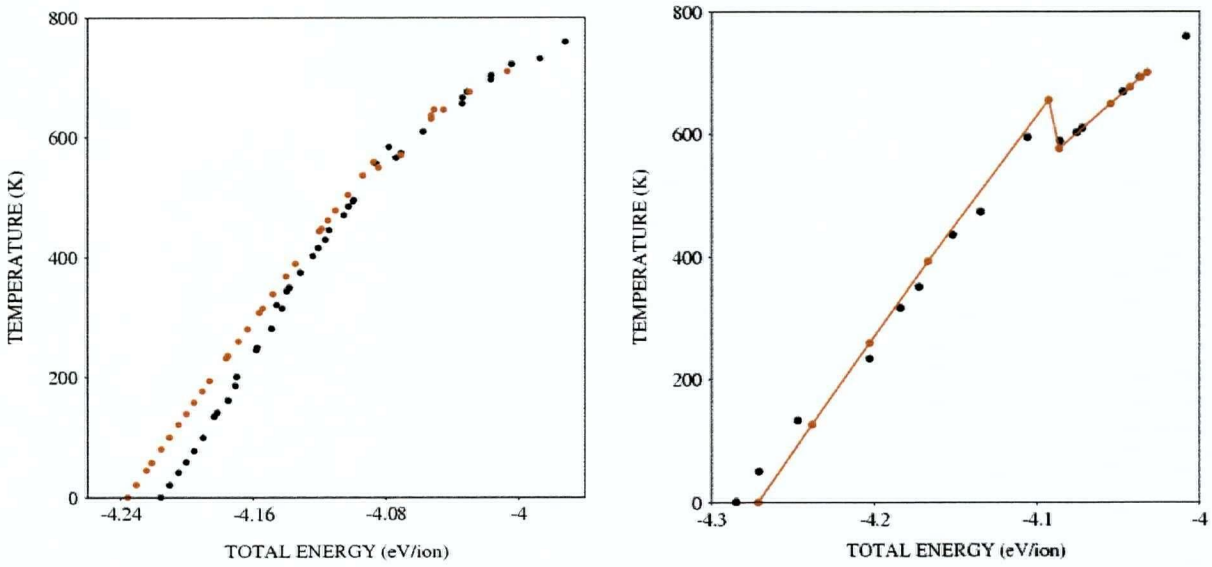

Figure 3.10: Caloric curves for $(LiCl)_{32}$ (left) and $(LiCl)_{108}$ (right). The black and red curves correspond respectively to separate heating and cooling curves. The unclear melting-freezing transition for $(LiCl)_{32}$ occurs at around -4.08eV/ion. The same transition occurs at $\simeq$ -4.1eV/ion for $(LiCl)_{108}$. A series of rearrangements occurs in both cases starting at -4.185eV/ion for $(LiCl)_{32}$ and at -4.25eV/ion for $(LiCl)_{108}$.

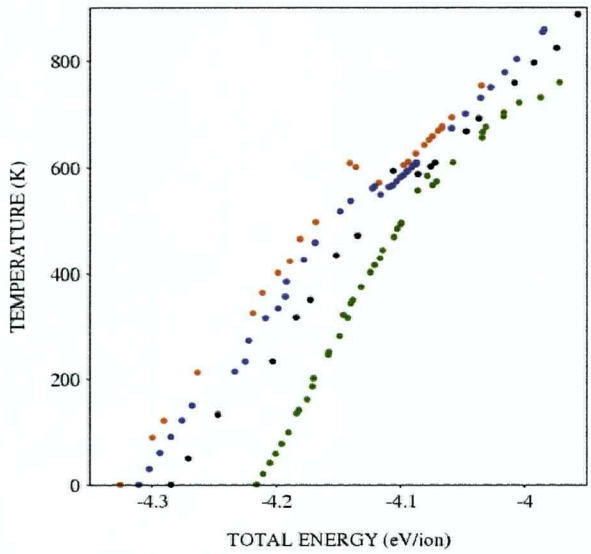

Figure 3.11: Caloric curves for $(LiCl)_{32}$ (green), $(LiCl)_{108}$ (black), $(LiCl)_{256}$ (purple) and $(LiCl)_{500}$ (red) obtained by heating the clusters. The melting occurs at around -4.1eV/ion in all four cases. Also, a series of rearrangements takes place at around -4.18eV/ion for $(LiCl)_{32}$ and at -4.25eV/ion for the other three larger clusters.

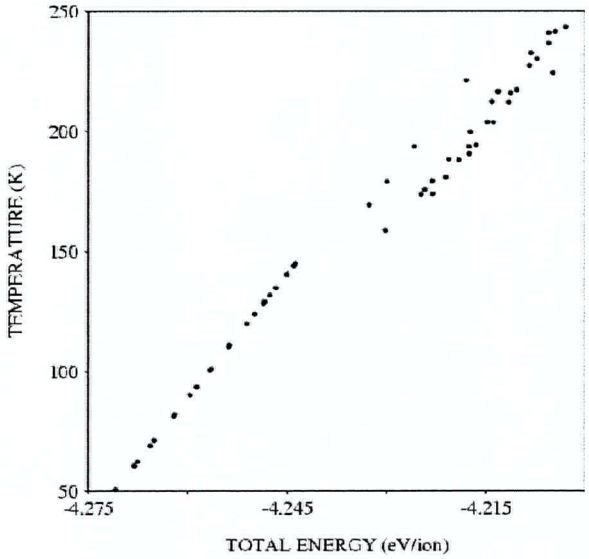

Figure 3.12: Multiple caloric curves for $(LiCl)_{108}$ starting with different initial conditions. The change in energy occurring at -4.24eV/ion corresponds to an entropy driven transition to an expanded ring structure.

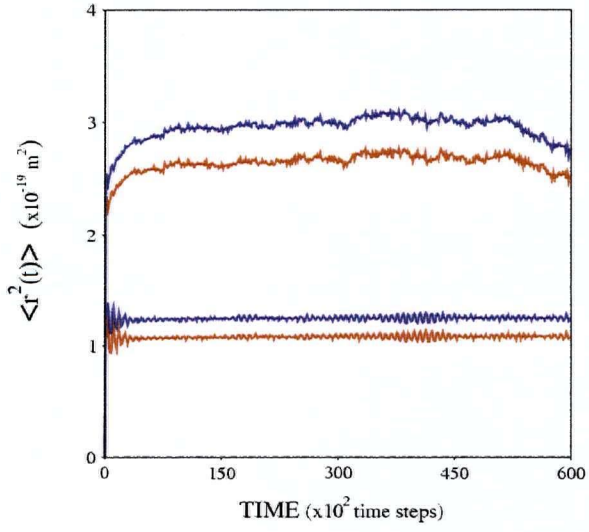

Figure 3.13: MSD curves at the low energy transition for $(LiCl)_{108}$. The bottom and upper curves are respectively taken before (-4.245eV/ion) and after (-4.225eV/ion) the first rearrangement. The purple and red lines correspond to the Li^+ and Cl^- ions.

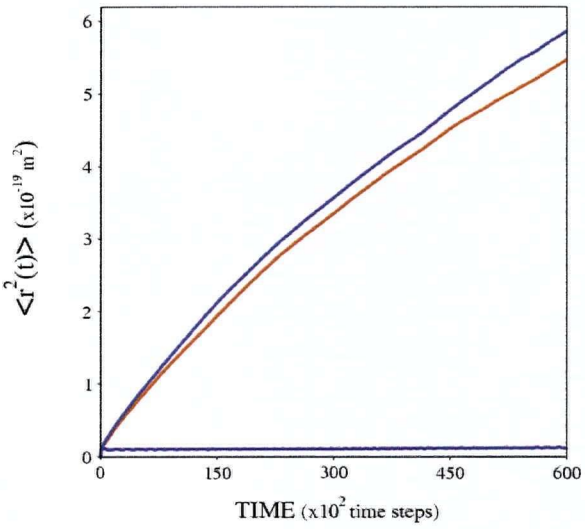

Figure 3.14: MSD curves at freezing for $(LiCl)_{108}$. The upper and lower curves were calculated just before (-4.086eV/ion) and after (-4.093eV/ion) freezing. The purple and red lines correspond to the Li^+ and Cl^- ions.

-4.09eV/ion for $(LiCl)_{108}$ show a clear separation between the solid and liquid structures. On the other hand, the solid and liquid structures at melting for $(LiCl)_{32}$, $(LiCl)_{256}$ and $(LiCl)_{500}$ are very similar in energy. This renders difficult the determination of the melting transition using the associated MSD curves (see Fig. 3.15 for an example). Moreover, the supposedly solid MSD curves do not have a null slope which means that the ions still have a lot of mobility (Fig. 3.15). This can be explained by the fact that for LiCl clusters there is no fixed lattice, so the difference in energy between the solid and liquid state is small. This hypotheses is also supported by the absence of a trend in the increase of the melting temperature as the size of the cluster increases (Fig. 3.11), whereas for KCl, the melting temperature clearly increases as a function of size (Fig. 3.6).

As mentioned earlier, of all the larger clusters only $(LiCl)_{32}$ led to a non-cubic low energy state. The final frozen structure formed was a nicely symmetric hollow cylinder whose surface was made of hexagonal rings (see Fig. 3.16 for snapshots). The series

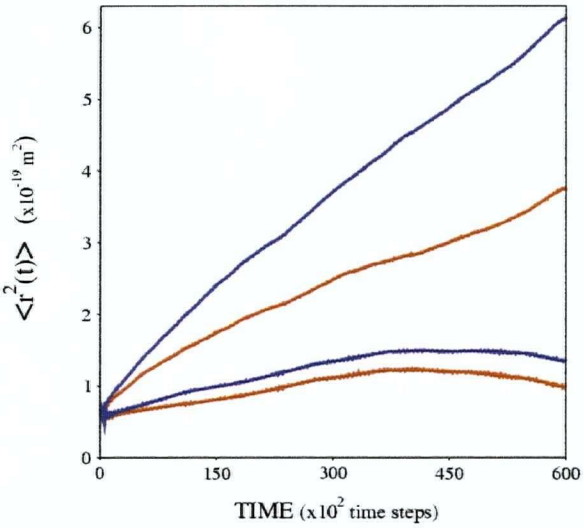

Figure 3.15: MSD curves at freezing for $(LiCl)_{32}$. The upper and lower curves were calculated just before (-4.071eV/ion) and after (-4.084eV/ion) freezing. The purple and red lines correspond to the Li^+ and Cl^- ions.

of rearrangements that occurred during heating can also clearly be observed from the distribution of ions around the center of mass (Fig. 3.17). The first rearranged structure shown in Fig. 3.17 still has ions near the center of mass whereas the final expanded structure has a null concentration of ions up to 3$\mathring{A}$ from the center of mass. This kind of hollow structure is also found in the case of $(LiCl)_{108}$ as no ions are present within 5$\mathring{A}$ of the center of mass (Fig. 3.18). Also note the clear change in the distribution pattern when the fcc structure transforms to the expanded structure. The distribution of ions for the liquid state is also shown in Fig. 3.18 to demonstrate re-establishment of ions everywhere in space after melting has occurred. As mentioned earlier, the hollow ring structure now has a higher energy than the fcc structure. The expanded ring structure obtained through rearrangements has a really remarkable shape (Fig. 3.19). An inside view from one end shows the alignment of the atoms at the surface as well as a clear empty space inside the surface. Moreover, upon examining the surface it is again observed

that the basic building block of such structure is the hexagonal ring.

From the results discussed above, it is clear that ring structures form the most stable geometry at least up to $(LiCl)_{32}$. Beyond $(LiCl)_{108}$, the fcc structure takes over and becomes the ground state configuration. Intermediate size clusters were produced to see if the crossover to the fcc structure occurs for clusters smaller than $(LiCl)_{108}$. It was found that between $(LiCl)_{32}$ and $(LiCl)_{108}$ the clusters presented various structures. But, for a fixed number of ions the cubic structure resembling that of a fraction of crystal lattice was never stable. Therefore, it seems that up to $(LiCl)_{108}$ the only stable cubic structures are the 2n x 2n x 2n magic number clusters. Conversely, all $(KCl)_n$ clusters preferentially have the rock salt structure as their ground state (see Fig. 3.1 and Fig. 3.9). The molten state of KCl and LiCl are no exceptions to the observed trend. For example, whereas the liquid state of $(KCl)_{108}$ is very compact, molten $(LiCl)_{108}$ gives rise to elongated rings and chains (Fig. 3.20) showing that the dipolar interactions are more important in LiCl.

The only larger clusters investigated beyond $(LiCl)_{108}$ were the two magic number clusters $(LiCl)_{256}$ and $(LiCl)_{500}$. At this size, the cubic character becomes more important due to a greater lattice, and the rearranged structures cannot expand as much as before. As a result, another entropy driven structural change occurred from hollow structures to more compact center-filled structures. Nevertheless, the strong dipolar character of LiCl still creates hexagonal rings in the rearranged structures. These last two clusters are very similar and can therefore be treated simultaneously by showing the structures of only one of them. Figure 3.21, which displays the distribution of ions for $(LiCl)_{500}$, does not show a clear gap at small distances as is the case for $(LiCl)_{108}$ (Fig. 3.18). In fact, near the melting transition the distribution of ions of the rearranged structure looks more like the liquid state which means that there are atoms almost everywhere in space. On the other hand, the distribution of ions after rearrangement occurs at -4.25eV/ion

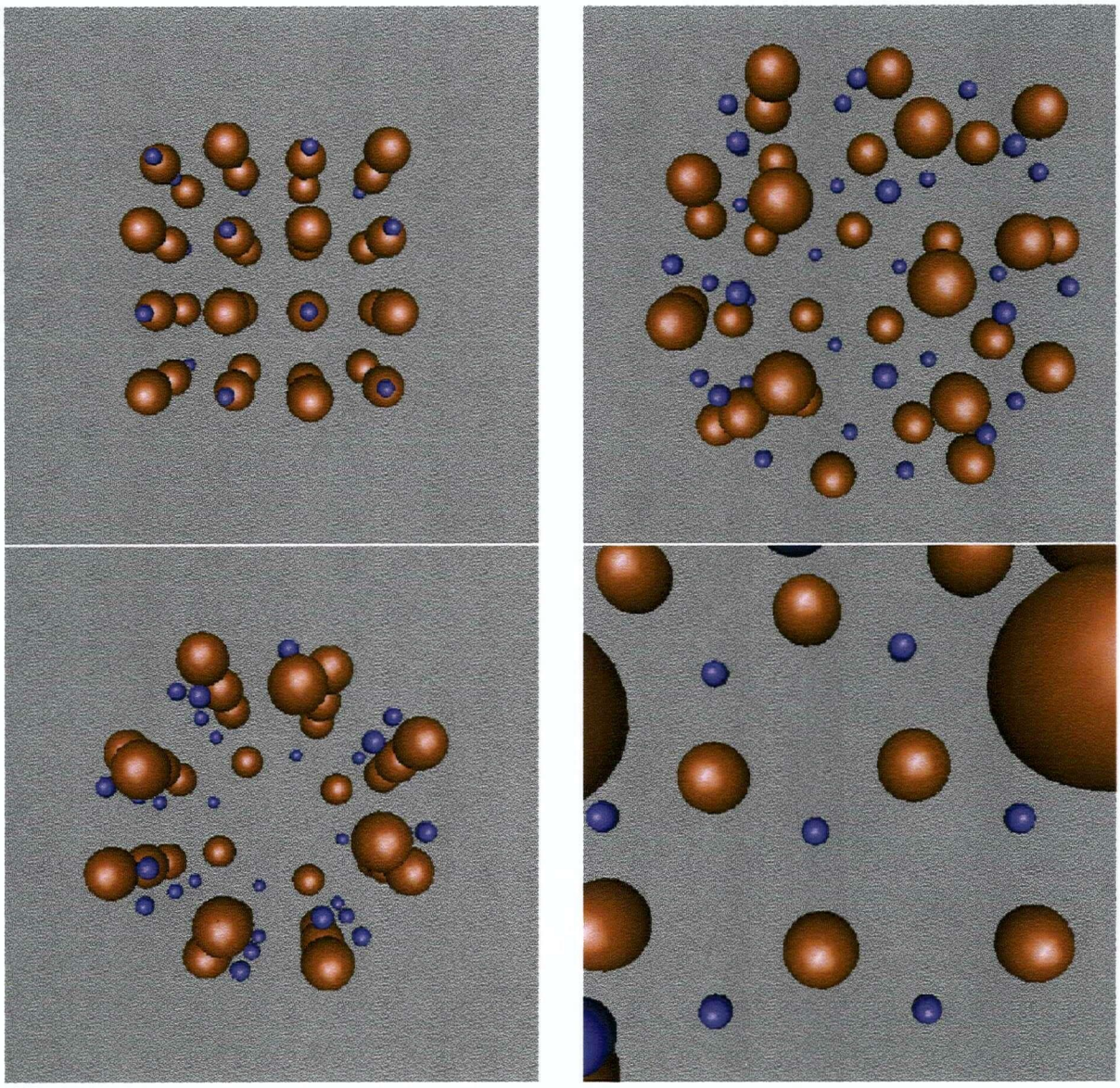

Figure 3.16: Snapshots of $(LiCl)_{32}$ during heating. Top left; initial fcc structure at -4.216eV/ion. Top right; first rearrangement at -4.184eV/ion. Bottom left; Lowest energy structure upon cooling to -4.236eV/ion. Bottom right; hexagonal rings on the surface of the low energy structure at -4.236eV/ion. The purple and red colours correspond to the Li^+ and Cl^- ions.

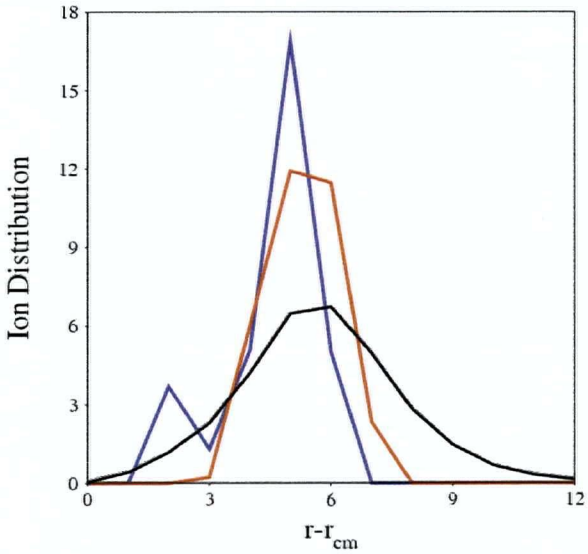

Figure 3.17: Ion distributions relative to the center of mass for $(LiCl)_{32}$. The purple, red and black lines correspond respectively to the first rearranged structure, the low energy hollow structure at -4.236eV/ion and a molten structure at -4.007eV/ion.

is clearly different from the distribution of ions in the fcc structure. Note that very few ions are present near the center of mass of the rearranged structure. This small gap in the distribution of ions is explained by the expansion of the structure as ring formation occurs, leaving greater distances between ions. The presence of rings inside of the structure is clearly observed from Fig. 3.22 which displays the series of events during heating. Note the resemblence of the rearranged structure to the liquid structure. It is therefore not surprising to see that weak melting transitions (see Fig. 3.9 and Fig. 3.10) are observed as the energies of the LiCl cluster structures before melting are very close to the energy of the molten state.

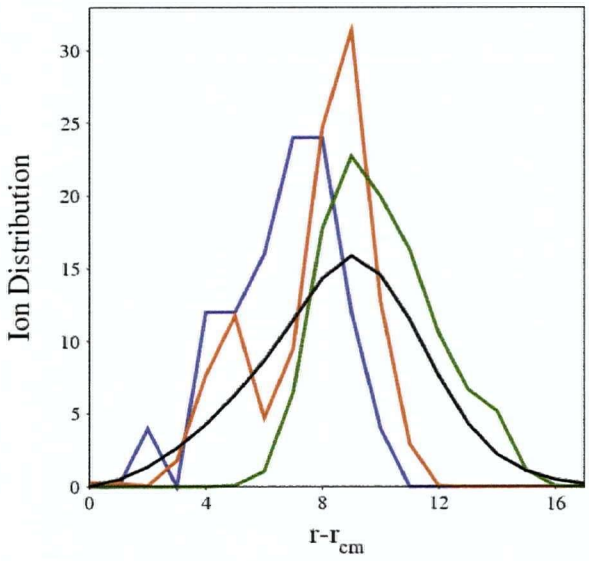

Figure 3.18: Ion distributions relative to the center of mass for $(LiCl)_{108}$. The purple, red, green and black lines correspond respectively to the fcc (-4.285eV/ion), first rearranged structure (-4.203eV/ion), low energy hollow structure (-4.271eV/ion) and a molten structure (-4.032eV/ion).

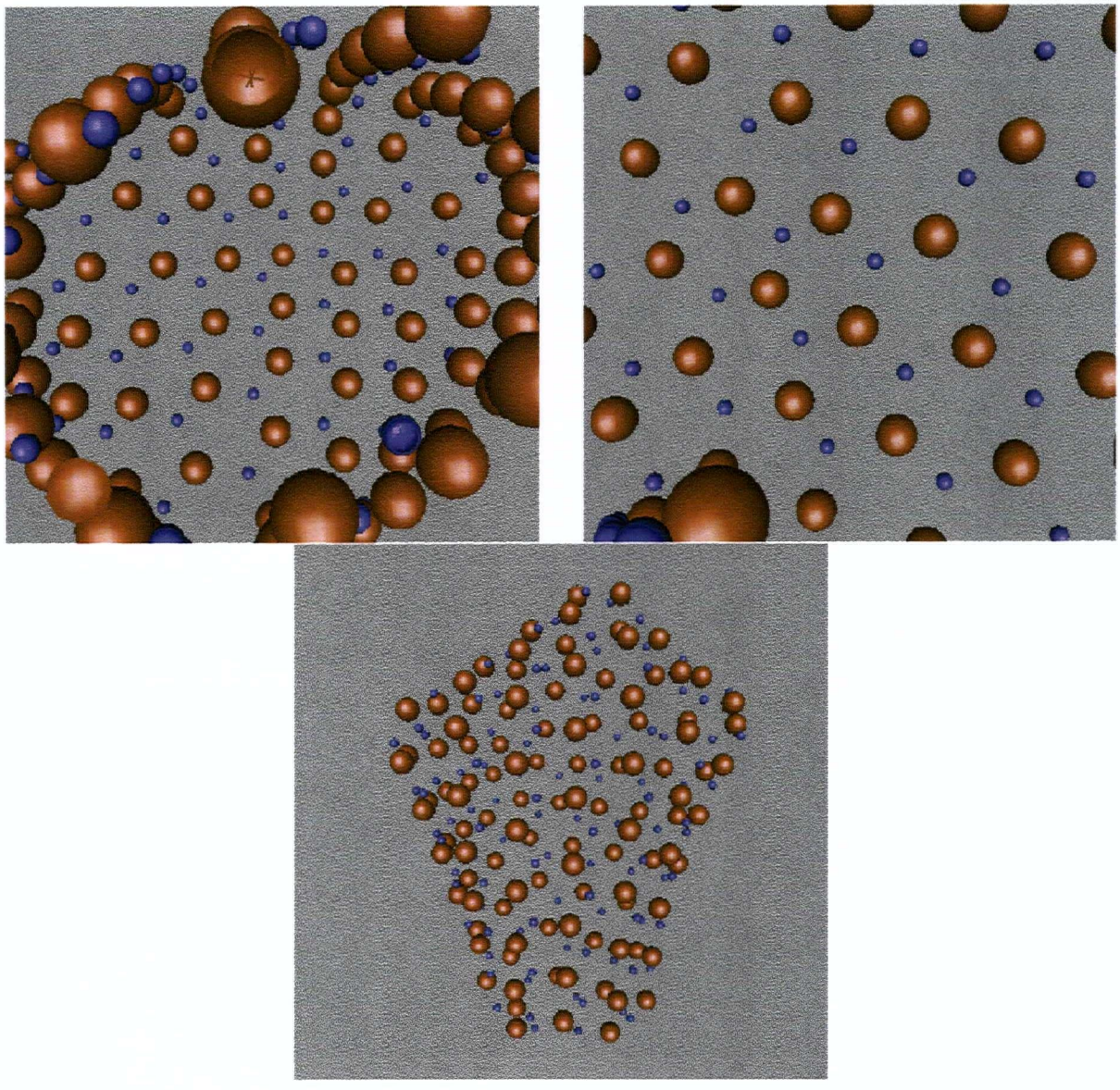

Figure 3.19: Snapshots of the hollow isomer of $(LiCl)_{108}$ at -4.271eV/ion. The top left image shows an inside view, the top right image shows the ring surface and the bottom image shows the overall structure of the isomer. The purple and red colours correspond to the Li^+ and Cl^- ions.

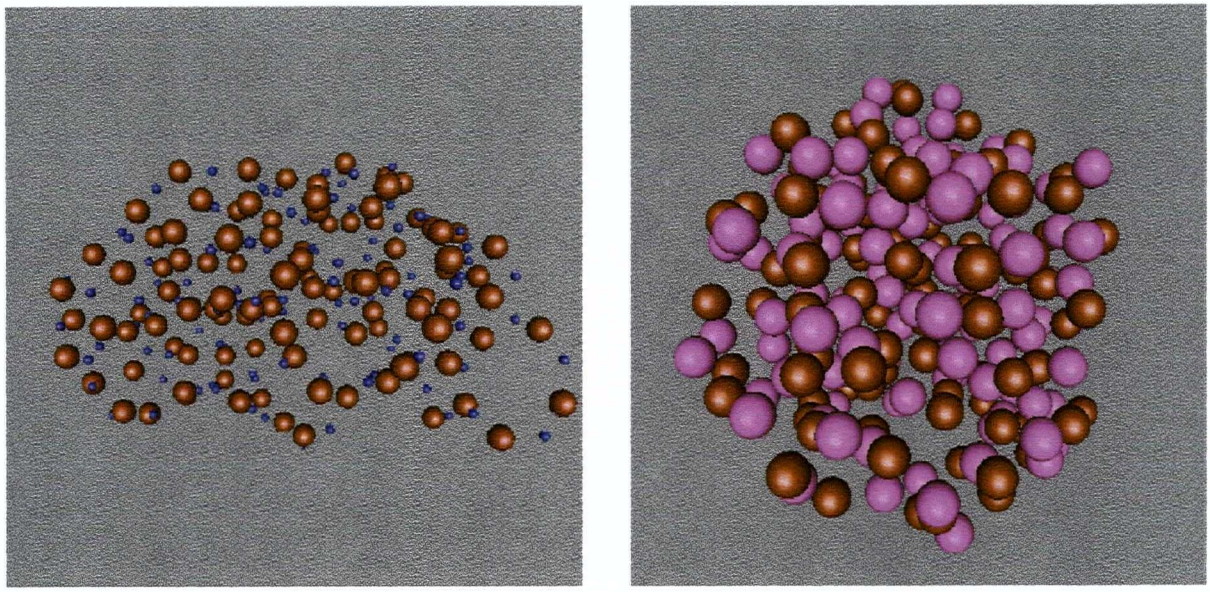

Figure 3.20: Snapshots of both $(LiCl)_{108}$ (left) and $(KCl)_{108}$ (right) in the liquid state taken respectively at -4.032eV/ion and -4.24eV/ion. The purple, red and pink colours correspond to the Li^+, Cl^- and K^+ ions.

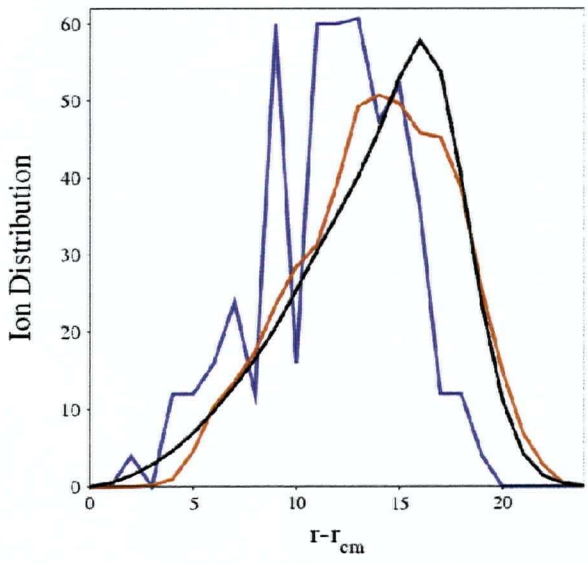

Figure 3.21: Ion distributions relative to the center of mass for $(LiCl)_{500}$. The purple, red and black lines correspond respectively to the fcc structure (-4.325eV/ion), rearranged structure just before melting (-4.136eV/ion), and a molten structure (-3.961eV/ion).

3.4 Mixtures:$(KCl)_n$-$(LiCl)_{108-n}$

In this section we present the results obtained for binary mixtures using the magic number clusters consisting of 8 and 216 ions. This allowed a significant range of concentrations to be studied (see Table 3.1), ranging from K-rich to Li-rich clusters. The size of the cluster was sufficiently large to give good statistics even for the low concentration regime which had reduced sampling possibility. Indeed, it allowed us to unravel some of the important structural details necessary to understand the behaviour of mixtures.

Firstly, as for the case of pure clusters, it is interesting to have a quick look at the various unit cells possible for mixtures using the first magic number cluster consisting of 8 ions. The caloric curves with 0.25, 0.5, and 0.75 LiCl mole fraction are all shown in Fig. 3.23. From these curves we can extract the low energy states which will later form the building blocks for larger clusters. Once again, different behaviour was observed. The

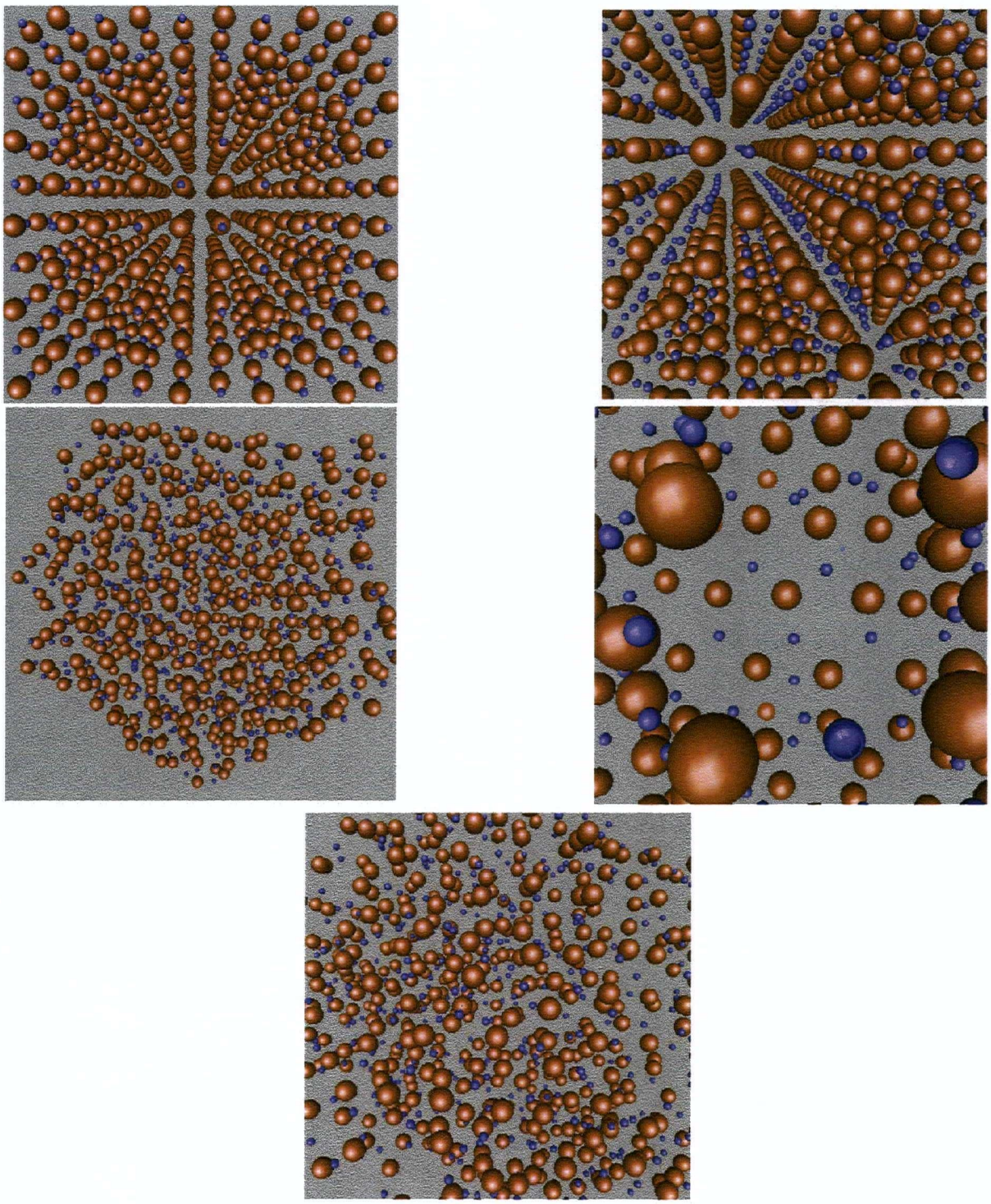

Figure 3.22: Snapshots of $(LiCl)_{500}$. First row: two different views of the initial fcc structure (-4.325eV/ion), second row: the presence of rings (right) in the expanded structure (left) before melting (-4.136eV/ion), third row: molten structure (-4.067eV/ion). The purple and red colours correspond to the Li^+ and Cl^- ions.

Table 3.4: A summary of the low energy structures obtained for the basic building blocks of mixtures and their associated energies. Note that some of the energies, marked by a *, were extrapolated to zero temperature. The energies are in eV/ion.

x_{LiCl}	cubic structure	ring structure
0.25	-3.405	-3.375*
0.5	-3.600	-3.585*
0.75	-3.784	-3.800*

energies of the low energy structures and low isomers are shown in Table 3.4. Clusters with LiCl mole fractions of 0.25 and 0.5 both underwent an entropy driven transition from a stable deformed cubic structure to a higher energy 8-membered ring structure (see Fig. 3.24 for snapshots). Conversely, the 0.75 LiCl mole fraction cluster gives an 8-membered ring upon rearrangement as the low energy structure (see Fig. 3.23 and 3.24). From these results we can already see that the KCl structure tends to dominate. Though, note that the 0.5 LiCl mole fraction cluster only favours a complex cube by a very slight energy difference. We will now see how this behaviour applies to larger mixtures.

For all runs, the cluster was started on a pure KCl fcc lattice. Substitution of some potassium ions was then made using a random number generator to obtained the desired LiCl mole fraction. The initial velocities were set to zero to have zero net linear and angular momentum. Then, the cluster was quickly heated up to a temperature well into the molten state. This was followed by cooling to obtain a stable frozen structure which is not necessarily the ground state. In some cases, the caloric curve was obtained by slowly heating the cluster to the molten state. Upon cooling the low energy configuration was always found to have a lower energy than the initial fcc structure as there are a large number of possibilities for the mixtures to arrange themselves (Fig. 3.26). Therefore, the caloric curve obtained by cooling was judged more relevant and was solely produced in most cases (Fig. 3.25 and 3.26).

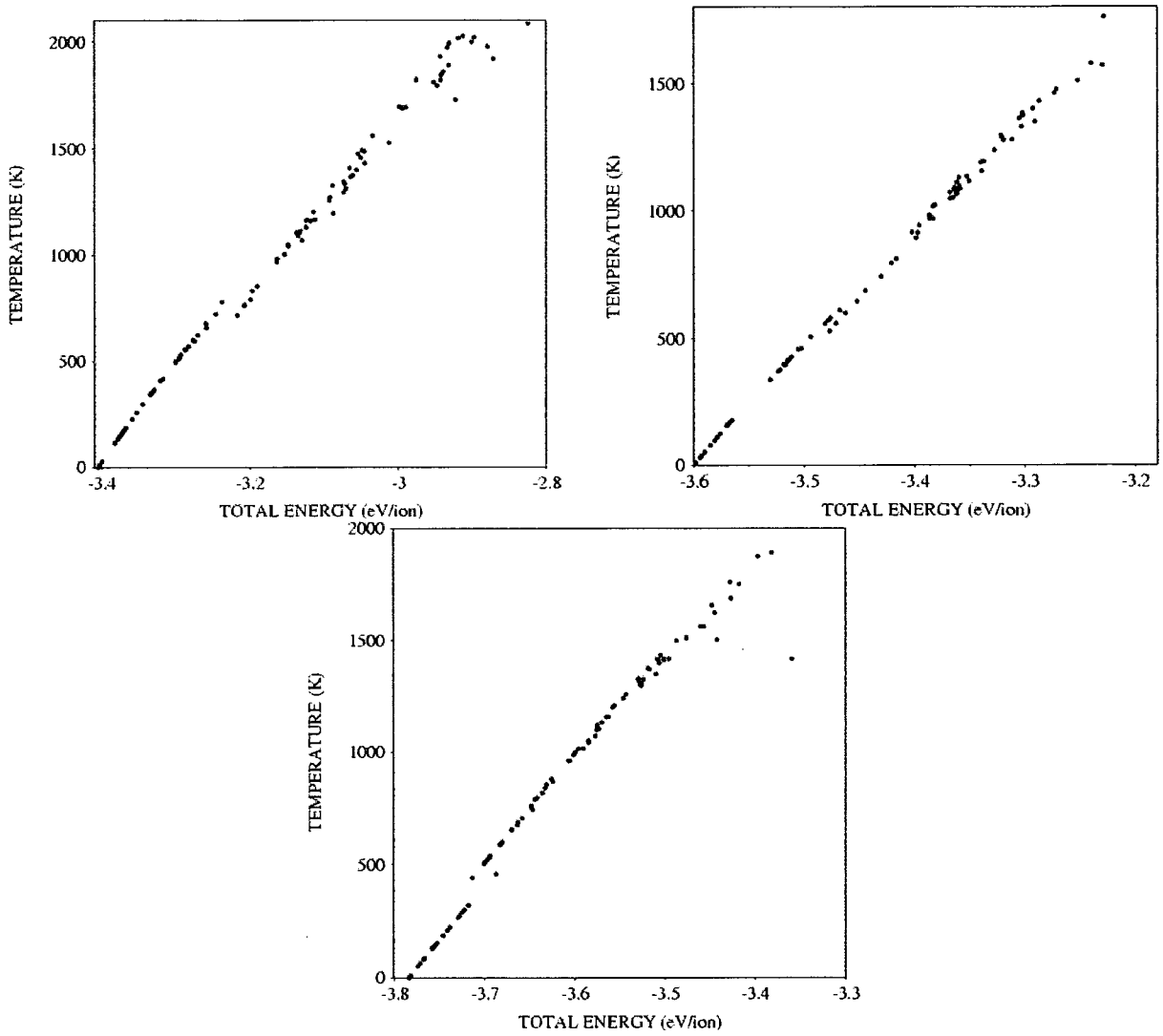

Figure 3.23: Caloric curves obtained by heating the three basic unit cells with 0.25 (top left), 0.5 (top right), and 0.75 LiCl mole fraction (bottom). In the top left curve, melting and evaporation occur at -3.22eV/ion and -2.9eV/ion, respectively. Similarly for the top right curve, melting and evaporation occur at -3.47eV/ion and -3.23eV/ion, respectively. For the bottom curve, a rearrangement to a more stable ring structure occurs at -3.7eV/ion followed by evaporation at -3.4eV/ion.

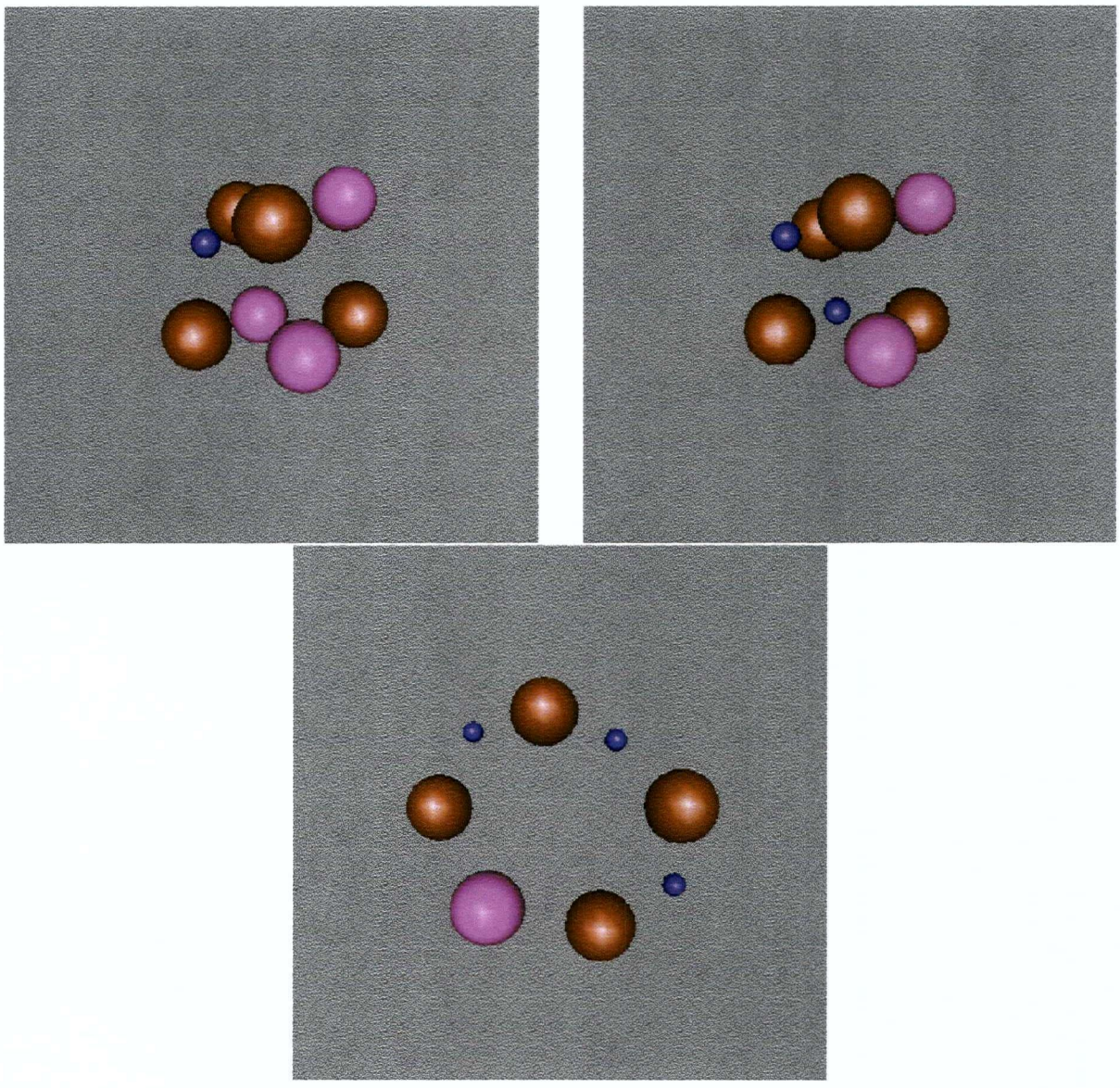

Figure 3.24: Snapshots of the three most stable basic unit cells with 0.25 (top left), 0.5 (top right), and 0.75 LiCl mole fraction (bottom). The purple, red and pink colours correspond to the Li^+, Cl^- and K^+ ions.

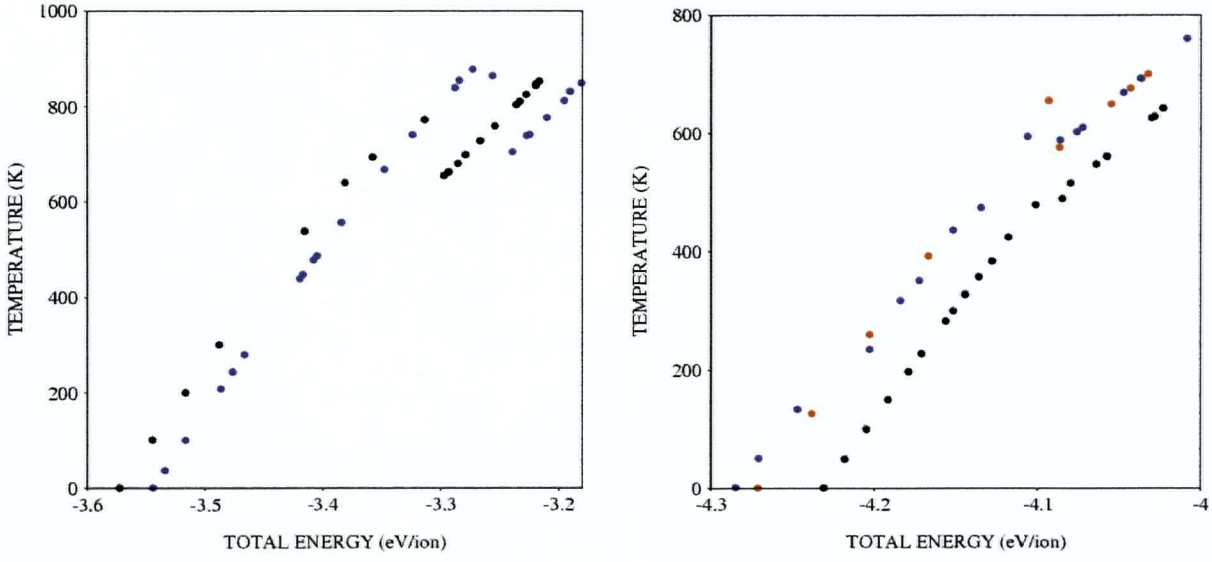

Figure 3.25: Caloric curves obtained by cooling (black) both 0.954 mole fraction KCl-rich (left) and LiCl-rich (right) clusters. The purple caloric curves correspond to the heating of the respective pure clusters, $(KCl)_{108}$ and $(LiCl)_{108}$. The red caloric curve corresponds to the cooling of pure $(LiCl)_{108}$. The melting-freezing transition of the KCl-rich, pure $(KCl)_{108}$ (left), and both the LiCl-rich, and pure $(LiCl)_{108}$ (right) occur respectively at -3.31eV/ion, -3.25eV/ion, and -4.1eV/ion.

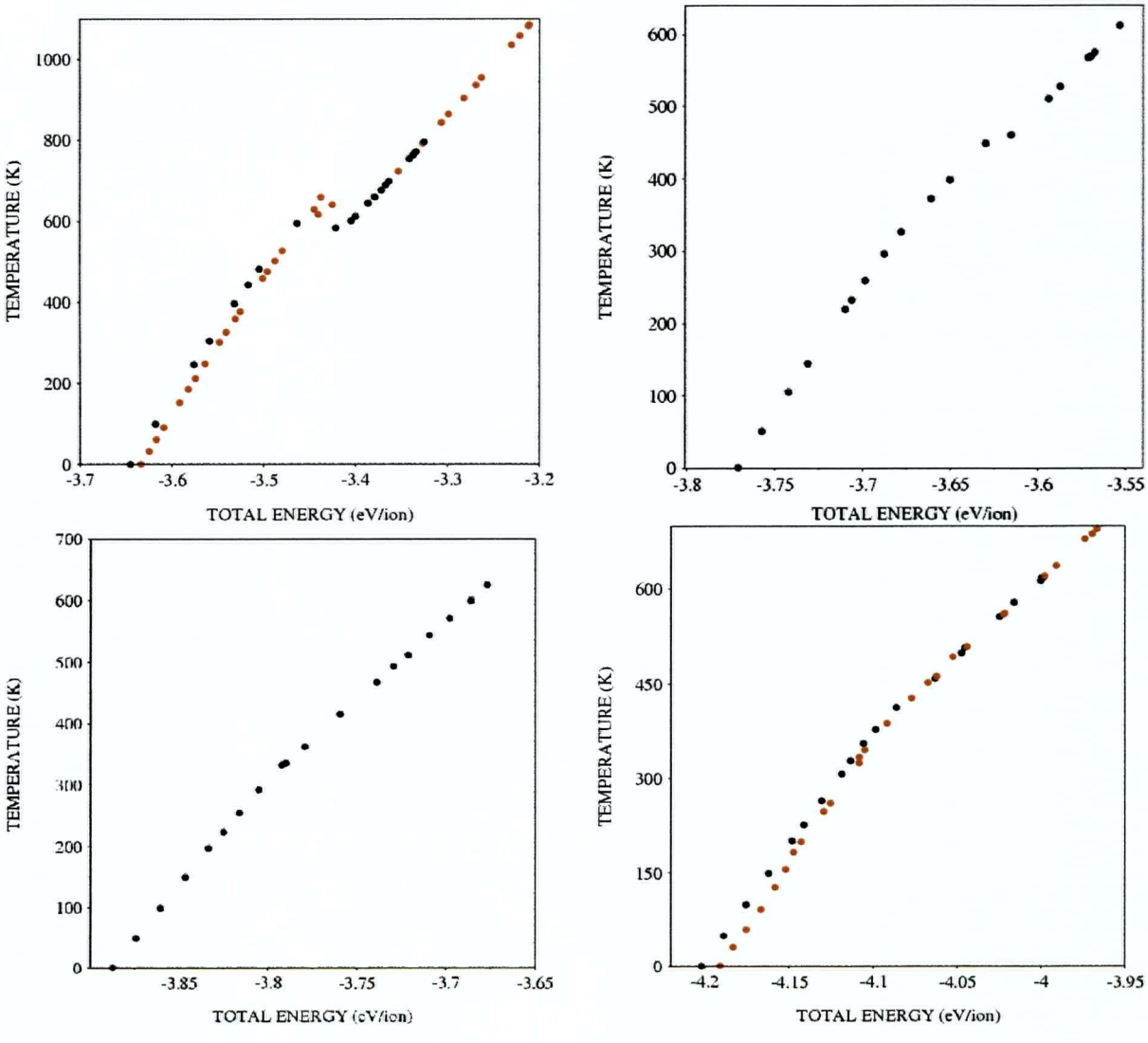

Figure 3.26: Caloric curves obtained by cooling (black) and heating (red) for the following KCl mole fractions: 0.852 (top left), 0.667 (top right), 0.509 (bottom left), and 0.093 (bottom right). In the same order, the melting-freezing transition occurs at -3.45eV/ion, -3.62eV/ion, -3.78eV/ion, and -4.1eV/ion.

Table 3.5: A summary of the energies obtained for the low energy structure of some mixtures made of 216 ions. The energies are in eV/ion.

x_{KCl}	Energy
1.0	-3.544
0.954	-3.572
0.852	-3.645
0.667	-3.771
0.509	-3.887
0.093	-4.202
0.046	-4.231
0.0	-4.285

The energies of the low energy structures and low isomers obtained for some mixtures are listed in Table 3.5. As seen from the caloric curves the behaviour of the mixtures differs significantly. At both extremes, the clusters with less than 0.05 LiCl or KCl mole fraction behave very similarly to the pure cases. Firstly, as for $(KCl)_{108}$, the caloric curve of the KCl-rich (0.954 KCl mole fraction) cluster has a very sharp freezing signature (Fig. 3.25) and freezes into the cubic structure (Fig. 3.27). Due to the stronger interactions of the Li^+ ions with the neighboring Cl^- ions, the melting-freezing transition (Fig. 3.25) of the K-rich cluster was shifted to a lower energy (-3.31eV/ion) compared to the pure $(KCl)_{108}$ cluster (-3.25eV/ion). As a result of the tendency of LiCl to form expanded ring structures (Fig. 3.16 and Fig. 3.19), ion segregation leaves all the Li^+ ions at the surface (Fig. 3.27). The same effect is observed from the distribution of ions (see Fig. 3.28) as no Li^+ ions are present at a distance less than $7\mathring{A}$ from the center of mass.

On the other hand, the freezing transition of the 0.954 LiCl mole fraction cluster occurs at the same energy as the pure $(LiCl)_{108}$ cluster, $\simeq$ -4.1 eV/ion (see Fig. 3.25). Moreover, its weak freezing signature is very similar to the melting signature obtained for the pure cluster. Accordingly, the same kind of hollow structure, made out of hexagonal rings, is observed (see Fig. 3.29). The ions are all positioned on the surface as indicated

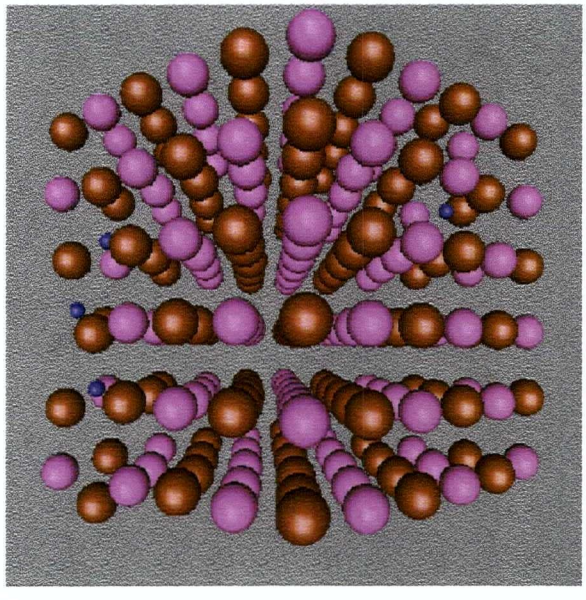

Figure 3.27: Snapshot of the low energy structure of $(KCl)_{103}$-$(LiCl)_5$ at -3.572eV/ion. The purple, red and pink colours correspond to the Li^+, Cl^- and K^+ ions.

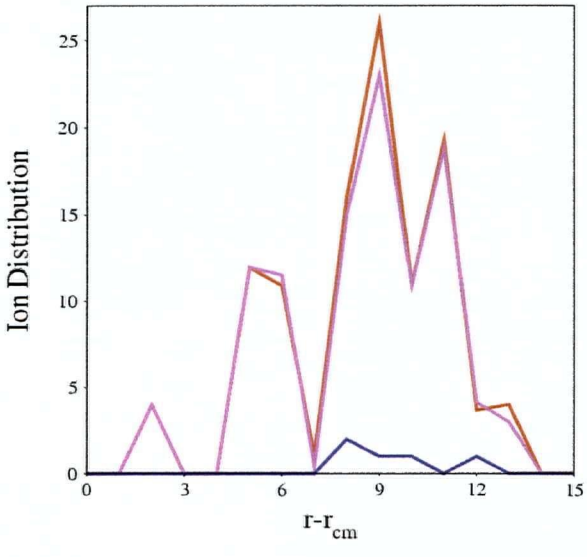

Figure 3.28: Ion distribution relative to the center of mass for $(KCl)_{103}$-$(LiCl)_5$ in the frozen fcc structure at -3.572eV/ion. The purple, red and pink lines correspond Li^+, Cl^- and K^+ ions.

by the distribution of ions relative to the center of mass (Fig. 3.30). In the liquid state, ions are found everywhere in space. Upon freezing, the ions move to the surface forming a much narrower distribution. This reorganization of the ions leaves a null concentration in the inside region, 0 to 6$\mathring{A}$ from the center of mass. The K^+ ions are all included in these rings but have more mobility on the surface than the Li^+ and Cl^- ions (as shown by the MSD curves at freezing) as they do not naturally form regular rings (Fig. 3.31).

For Li-rich and K-rich clusters with mole fractions less than 0.954, the pure character starts to disappear. Indeed, in the K-rich case, as the KCl mole fraction is decreased the sharpness of the freezing transition slowly reduces. The transition is still easily observable at 0.852 and 0.667 KCl mole fraction (Fig. 3.26), but below this value, down to 0.093 KCl mole fraction, it becomes hardly discernible. For example, at 0.509 KCl mole fraction the signature comes down to two closely connected dots at -3.78eV/ion (Fig. 3.26). At 0.093 KCl mole fraction the change of phase at -4.1eV/ion is faintly marked by a small change in the respective slopes of the liquid and solid parts of the caloric curve (Fig. 3.26). The absence of sharp melting for all clusters in that region (from 0.667 to 0.093 KCl mole fraction) suggests that the freezing process, as observed by the caloric curves, is not sharp but rather continuous and spreads over a certain range of temperature. This means that the energies of the solid and liquid structures are very similar.

The low energy structures obtained for the clusters having KCl mole fraction of 0.852, 0.667, 0.509, and 0.093 are displayed in Fig. 3.32. At a 0.852 KCl mole fraction, the final structure associated with the end of the cooling part of the caloric curve (Fig. 3.26) does not have a completely symmetric rock salt structure as the lowest energy state (see Fig. 3.32 and Table 3.4). Instead, as a result of ion segregation the symmetry is disrupted by the formation of two expanded Li-rich regions at the surface. The distribution of ions relative to the center of mass shows this trend as there are no Li^+ ions at a distance less than 5$\mathring{A}$ from the center of mass (Fig. 3.33). Moreover, due to ion segregation it is now

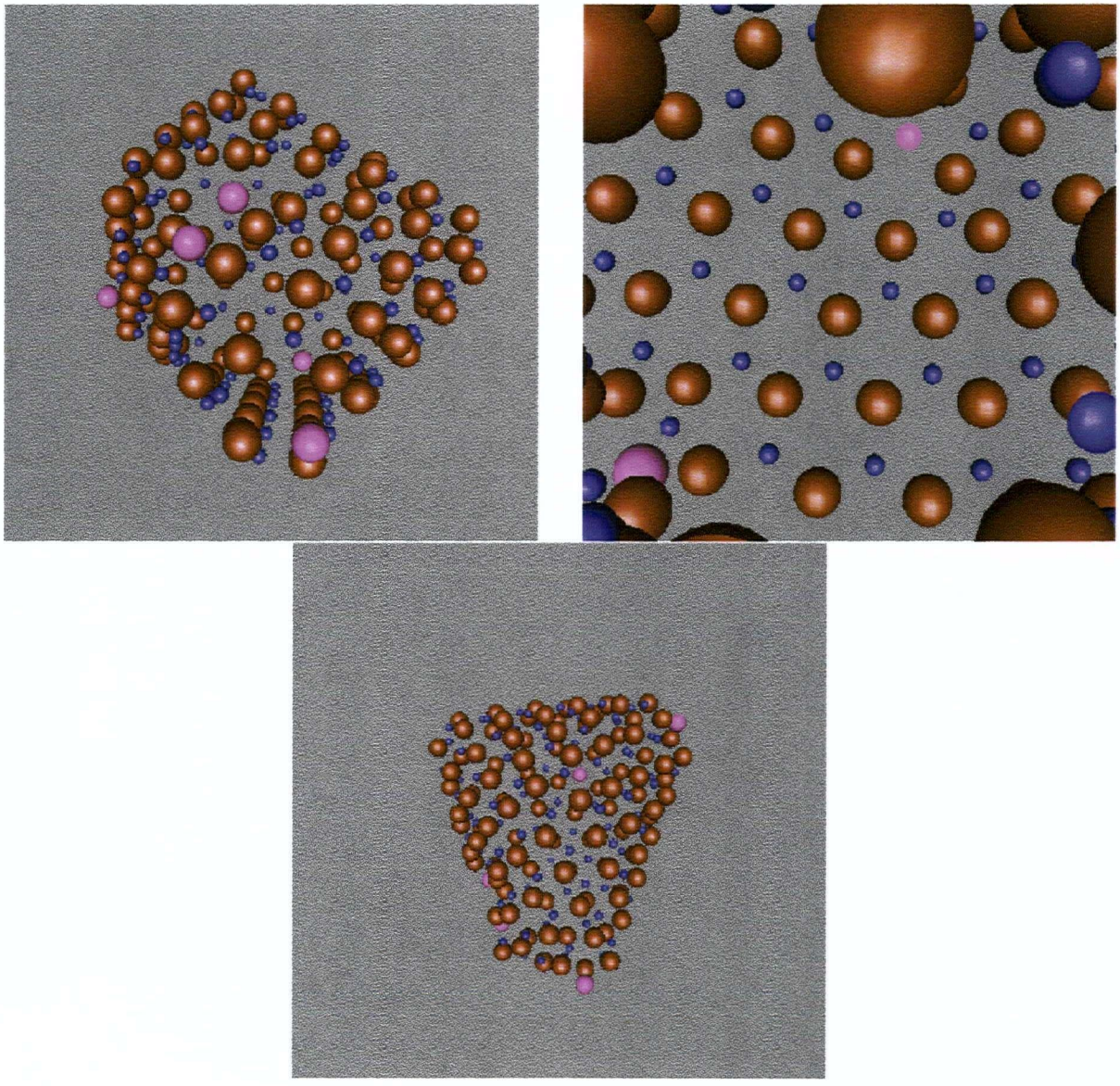

Figure 3.29: Snapshots of $(KCl)_5$-$(LiCl)_{103}$ at -4.231eV/ion. The top left image shows the alignment of the ions on the surface structure, the top right image shows an inside view of the ring surface, and the bottom image shows the overall hollow structure. The purple, red and pink colours correspond respectively to the Li^+, Cl^- and K^+ ions.

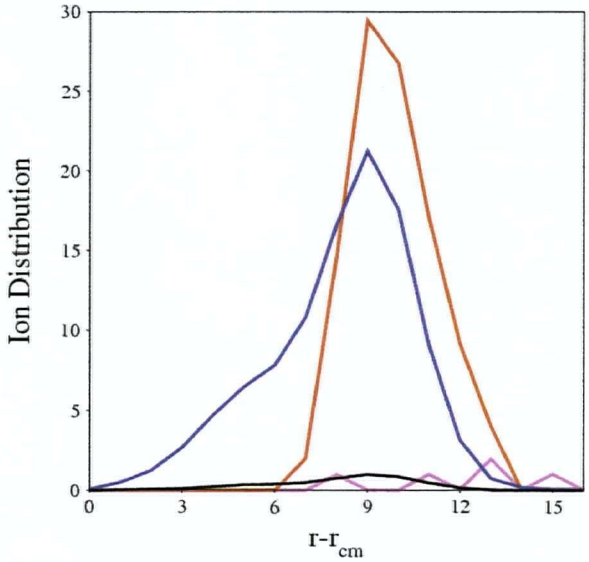

Figure 3.30: Ion distributions relative to the center of mass for $(KCl)_5$-$(LiCl)_{103}$. The red (Li^+ and Cl^-) and pink (K^+) lines correspond to the solid structure at -4.231eV/ion. The purple (Li^+ and Cl^-) and black (K^+) correspond to the molten state at -4.028eV/ion.

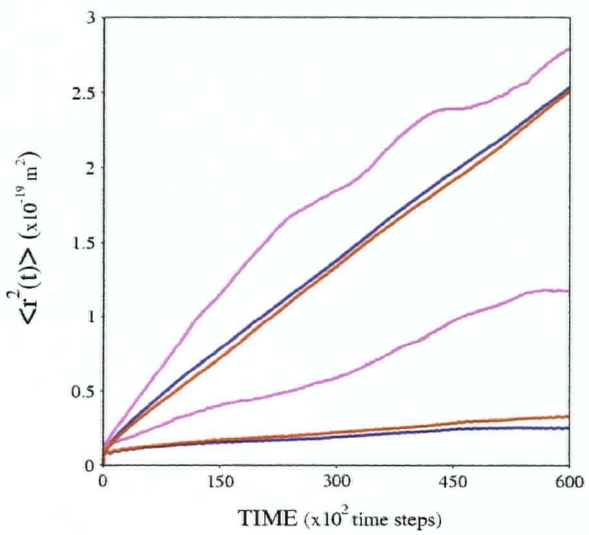

Figure 3.31: MSD curves at freezing for $(KCl)_5$-$(LiCl)_{103}$. The three top and three bottom lines correspond respectively to the liquid (-4.085eV/ion) and solid (-4.101eV/ion). The purple, red and pink colours correspond to the Li^+, Cl^- and K^+ ions.

possible to observe sequential melting of the different species. According to the caloric curve (Fig. 3.26), at -3.47eV/ion the cluster is supposed to be in the solid state. But, from the MSD curves (Fig. 3.34), only the K^+ ions are frozen. As in the pure case, a clear change in the mobility of the K^+ ions was observed upon freezing. At the same energies, the mobilities of the Li^+ and Cl^- ions are much greater than that of the K^+ ions. One must lower the energy further to observe the same frozen state for the Li^+ and Cl^- ions as pure LiCl freezes at a lower temperature. Note that the mobility of the Cl^- ions is strongly influenced by the Li-rich region. The small size and mass of the Li^+ ions give them even more mobility than the other two species in the liquid state (Fig. 3.34).

Even at a KCl mole fraction lower than 0.667, segregation is still very apparent from the structure of the frozen cluster which has a cubic portion in it next to a larger portion made of highly disordered cubic structures (see Fig. 3.32). Recall that the freezing signature in the caloric curve (Fig. 3.26), at energy -3.65 eV/ion, has now almost completely disappeared as the overall structure looks more like a disordered liquid structure with nearly the same energy at melting.

Up to now we have seen that as the LiCl mole fraction is increased the structure of the solid state becomes less and less ordered and its energy gets closer and closer to the energy of the liquid state. At a KCl mole fraction of 0.509, ion segregation is no longer observed. This cluster is one of the most useful in explaining the disappearance of the melting-freezing transition (Fig. 3.26). Its solid structure is a complex composition of the 0.5 KCl mole fraction deformed unit cell seen in Fig. 3.24. The only difference between the solid and liquid structures lies in the compactness (Fig. 3.35). Therefore, there is very little energy difference between solid and liquid ($\simeq$0.005eV/ion), which explains the observed continuous melting and the very faint change of energy upon freezing. Further evidence of a continuous melting-freezing process is obtained from the MSD curves. In order to observe the freezing of the cluster using the MSD curves (Fig. 3.36) it is necessary to

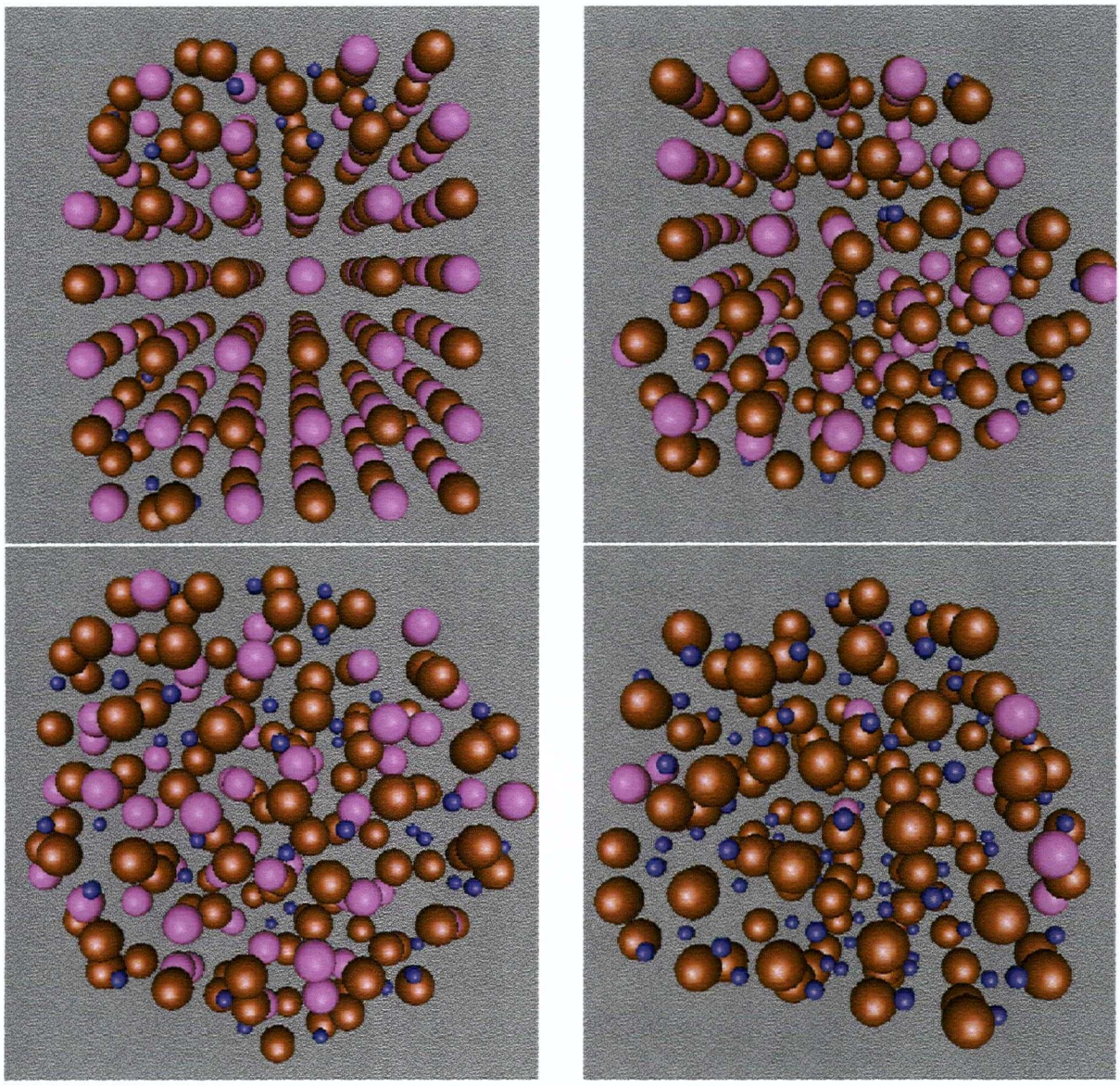

Figure 3.32: Snapshots of the low energy structures obtained for clusters with the following KCl mole fractions: 0.852 (top left), 0.667 (top right), 0.509 (bottom left), and 0.093 (bottom right). The purple, red and pink colours correspond Li^+, Cl^- and K^+ ions.

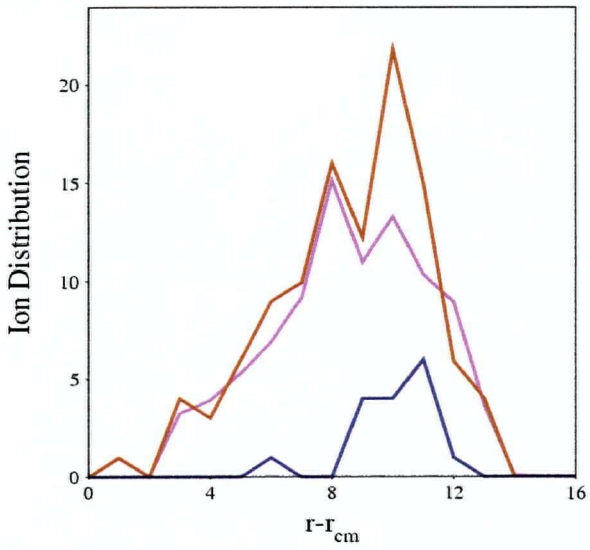

Figure 3.33: Ion distributions relative to the center of mass for $(KCl)_{92}$-$(LiCl)_{16}$ (0.852 KCl mole fraction) in the frozen structure at 3.645eV/ion. The purple, red and pink lines correspond to the Li^+, Cl^- and K^+ ions.

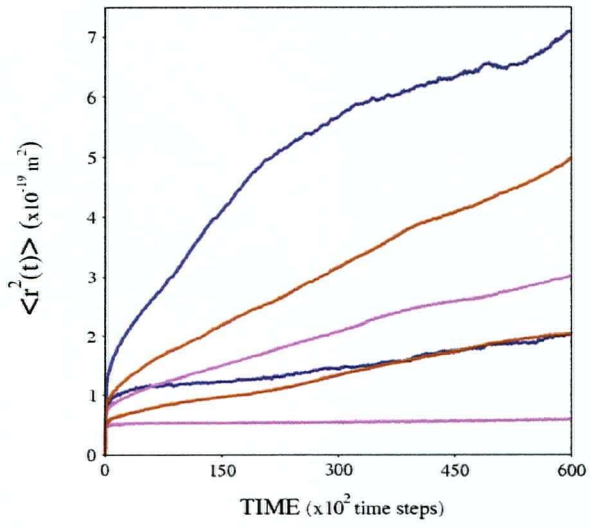

Figure 3.34: MSD curves at freezing for $(KCl)_{92}$-$(LiCl)_{16}$. The three top and three bottom lines correspond respectively to the liquid (-3.386eV/ion) and solid (-3.645eV/ion). The purple, red and pink lines correspond to the Li^+, Cl^- and K^+ ions.

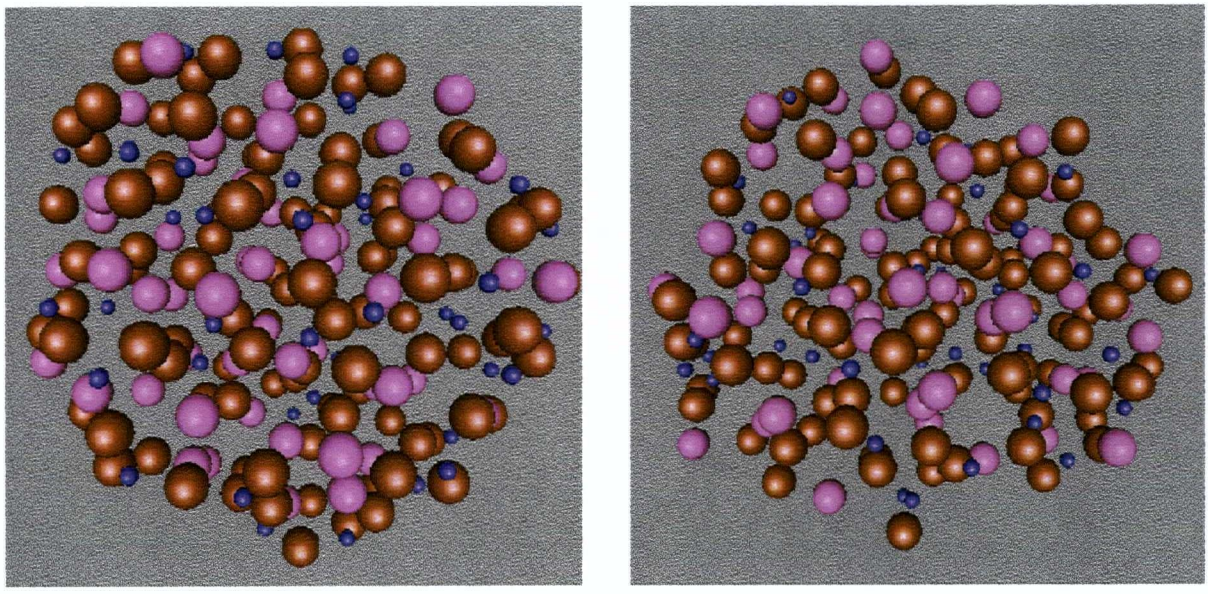

Figure 3.35: Snapshots of $(KCl)_{55}$-$(LiCl)_{53}$ in the solid state at -3.887eV/ion (left) and in the liquid state (right) at -3.760eV/ion. The purple, red and pink colours correspond to the Li^+, Cl^- and K^+ ions.

use data above and below the transition, at -3.775eV/ion and -3.805eV/ion, respectively (Fig. 3.26).

It is only when the LiCl mole fraction reaches 0.907 that rings start to appear in the cluster's solid structure (Fig. 3.32). However, they are still difficult to observe. One indirect way to observe them is by the clear alignment of either the Li^+ or Cl^- ions (bottom right section in Fig. 3.32). This alignment was also easily observed in the ring structure of $(LiCl)_{108}$ (Fig. 3.19). A chain is also easily seen in the liquid structure (Fig. 3.37). But still the liquid and solid structures are very similar in energy which explains why there is only a small change in the slope to indicate freezing at -4.1eV/ion (see Fig. 3.26).

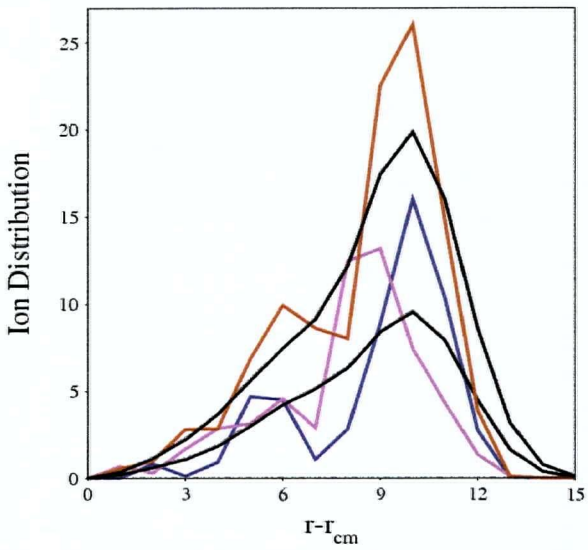

Figure 3.36: Ion distributions relative to the center of mass for $(KCl)_{55}$-$(LiCl)_{53}$ in the frozen structure at -3.887eV/ion and in the molten state at -3.686eV/ion. The purple, red and pink lines correspond to the Li^+, Cl^- and K^+ ions.

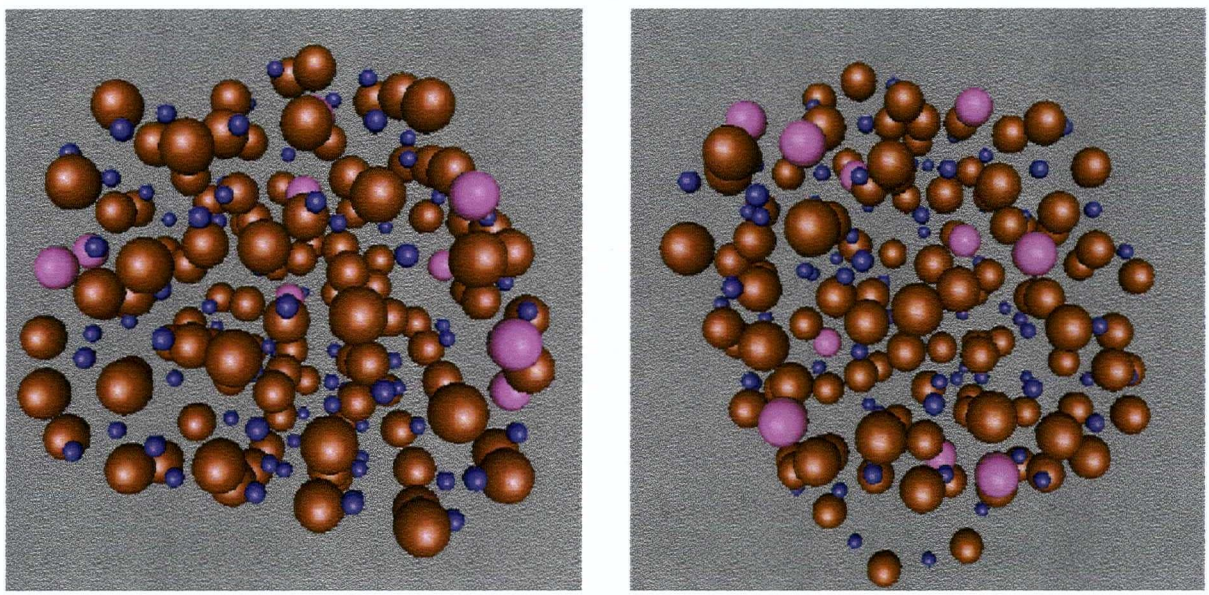

Figure 3.37: Snapshots of $(KCl)_{10}$-$(LiCl)_{98}$ in the low energy structure at -4.202eV/ion (left) and in the liquid state (right) at -4.00eV/ion. The purple, red and pink colours correspond to the Li^+, Cl^- and K^+ ions.

Chapter 4

Summary and Conclusions

This thesis is mainly directed towards elucidating the structural behaviour of strongly size-asymmetric alkali halide clusters at the melting and freezing transition. MD simulations were the sole technique employed in this investigation. This method allowed us to get interesting structural information in the case of pure LiCl clusters. The results obtained for small pure LiCl and KCl clusters clearly demonstrate different behaviours; small LiCl clusters undergo rearrangement to low energy ring structures, and small KCl clusters prefer to form cubic structures. The cause of this different behaviour is attributed to the relative importance of the dipolar character of the KCl and LiCl pairs. On one hand, the smaller contribution of the higher order terms in the multipole expansion for LiCl compared to KCl increases the importance of its dipolar character and gives rise to stable ring structures. On the other hand, small KCl clusters are less governed by their dipolar character and form cubic structures.

As a way of comparing the different behaviours, larger magic number LiCl and KCl clusters were studied. As expected, large KCl clusters, $(KCl)_{32}$ and $(KCl)_{108}$, exhibit sharp melting and freezing transitions with hysteresis and practically no phase coexistence. On the other hand, large LiCl clusters did not exhibit sharp melting/freezing transitions, except for the freezing transition of $(LiCl)_{108}$. Instead, due to the strong dipolar character in LiCl, larger clusters underwent a series of rearrangements during heating to finally melt from a less ordered expanded structure made out of hexagonal rings.

The structural study of $(LiCl)_{16}$ was our first new piece of information in the investigation of the interesting behaviour associated with LiCl. The low energy structure obtained in this case upon rearrangement was a hollow ball whose surface was made of rings. The second largest magic number cluster, $(LiCl)_{32}$, also underwent rearrangement to a low energy non-cubic structure. Again, ring formation led to a hollow cylindrical structure with lower energy than the regular cubic (fcc) structure. The creation of these hollow structures was encountered for cluster sizes as large as $(LiCl)_{108}$. However, the structural transformation occurring for $(LiCl)_{108}$ led to a higher energy ring structure. This means that the structural rearrangement was entropy driven. In the two larger clusters, $(LiCl)_{256}$ and $(LiCl)_{500}$, starting from the low energy cubic structure, entropy driven rearrangements still take place and produce higher energy center-filled ring structures. Thus, from these results it is observed that the strong dipolar character of LiCl creates a clear competition between ring-like and cubic structures. The rearrangements that take place during heating in all LiCl clusters lead to less ordered expanded ring structures with energies very similar to that of the liquid state, explaining the absence of a sharp melting. Accordingly, the strong dipolar character of LiCl decreases the energy difference between the solid and liquid phases which possibly explains the early melting of LiCl when compared to the other alkali halide salts.

The results obtained for the mixtures cover a large range of different behaviours going from pure KCl to pure LiCl behaviour. At both ends, mixtures containing less than 0.05 mole fraction of one of the species behave as in the pure case. Thus, $(KCl)_{103}$-$(LiCl)_5$ and $(KCl)_5$-$(LiCl)_{103}$ both have a cubic structure as their ground state and the Li-rich cluster rearranges to an expanded ring structure similar to $(LiCl)_{108}$ before melting. At greater KCl and LiCl mole fractions the clusters start to lose their pure properties. The strong cubic character of KCl is dominant over the strong dipolar character of LiCl over a wide range of concentrations; ion segregation produced some cubic portions in the low

energy structure for KCl mole fractions as large as 0.67. On the other hand, ring-like structures only start to be present for LiCl mole fractions greater than 0.9. The remaining intermediate compositions, from 0.67 to 0.1 KCl mole fraction, are characterized by a mixture of irregular cubic structures resembling that of the liquid structure with very small energy differences. This renders difficult the determination of the melting/freezing transition. These results indicate the insensitivity of the structures to LiCl concentration for a broad range of composition.

Bibliography

[1] J. Jellinek, T. Beck, and R. S. Berry. *J. Chem. Phys.*, 84:2783, 1986.

[2] J. D. Honeycutt and H.C. Anderson. *J. Phys. Chem.*, 91:4950, 1987.

[3] J. E. Adams and R. M. Stratt. *J. Chem. Phys.*, 93:1332, 1990.

[4] F. H. Stillinger and D. K. Stillinger. *J. Chem. Phys.*, 93:6013, 1990.

[5] D. O. Welch, O. W. Lazareth, G. J. Dienes, and R. D. Hatcher. *J. Phys. Chem.*, 64:835, 1976.

[6] T. P. Martin. *J. Chem. Phys.*, 67:5207, 1977.

[7] J. Luo, U. Landman, and J. Jortner. *Physics and Chemistry of Small Clusters.* NATO ASI Series B (Plenum, New York), 1987.

[8] N. G. Phillips, C. W. S. Cononver, and L. A. Bloomfield. *J. Chem. Phys.*, 94:4980, 1991.

[9] L. F. Fried and S. Mukamel. *Phys. Rev. Lett.*, 66:2340, 1991.

[10] N. H. Kaukonen, U. Landman, and C.L. Cleveland. *J. Chem. Phys.*, 95:4997, 1991.

[11] E. W. Draeger, J. C. Grossman, A. J. Williamson, and G. Galli. *J. Chem. Phys.*, 120:10807, 2004.

[12] I. L. Li and Z. K. Tang. *J. Appl. Phys.*, 95:6364, 2004.

[13] A.S. Clark and G. N. Patey. *J. Chem. Phys.*, 100:2213, 1994.

[14] M. L. Huggins and J. E. Mayer. *J. Chem. Phys.*, 1:643, 1933.

[15] L. Pauling. *J. A. C. S.*, 50:1036, 1928.

[16] F. G. Fumi and M. P. Tosi. *J. Phys. Chem. Solids*, 25:31, 1964.

[17] J. E. Campana, T. M. Barlak, R. J. Colton, J. J. De Corpo, J. J. Wyatt, and B. I. Dunlap. *Phys. Rev. Lett.*, 47:1046, 1981.

[18] T. M. Barlak, J. J. Wyatt, R. J. Colton, J. J. De Corpo, and J. E. Campana. *J. Am. Chem. Soc.*, 104:1212, 1982.

[19] O. Echt, K. Sattler, and E. Recknagel. *Phys. Rev. Lett.*, 47:1121, 1981.

[20] R. Pflaum, K. Sattler, and E. Recknagel. *Surf. Sci.*, 156:165, 1985.

[21] C. W. S. Conover, Y. A. Yang, and L. A. Bloomfield. *Phys. Rev. B*, 38:3517, 1988.

[22] Y. T. Twu, C. W. S. Conover, Y. A. Yang, and L. A. Bloomfield. *Phys. Rev. B*, 42:5306, 1990.

[23] P. C. R. Rodrigues and F. M. S. Silva Fernandes. *Int. J. Quantum. Chem.*, 84:169, 2001.

[24] A. Aguado, A. Ayuela, J. M. Lopez, and J. A. Alonso. *Phys. Rev. B*, 56:15353, 1997.

[25] A. S. Clarke and G. N. Patey. *J. Chem. Phys.*, 100:2213, 1993.

[26] C. G. Gray and K. E. Gubbins. *Theory of Molecular Fluids.* Clarendon Press, Oxford, 1984.

[27] D. Inman and S. H. White. *Molten Salt Electrolysis in Metal Production.* The Institution of Mining and Metallurgy, 1977.

[28] P. Faugeras, A. Lecocq, M. Hery, and M. Israel. *Note C. E. A.*, 1N:1963, 1975.

[29] D. L. Barney. *Argonne Nat. Lab. Report*, ANL:75, 1980.

[30] A. Aguado and P. A. Madden. *J. Chem. Phys.*, 117:7659, 2002.

[31] F. F. Abraham et al. *Nature*, 426:141, 2003.

[32] M. P. Allen and D. J. Tildesly. *Computer Simulation of Liquids.* Clarendon Press, 1989.

[33] T. L. Hill. *Introduction to Statistical Thermodynamics.* Dover Publications, Inc, 1986.

[34] C. Ochsenfeld, R. Ahlrichs, and Ber. Bunsenges. *Phys. Chem.*, 98:34, 1994.

[35] J. P. Rose and R. S. Berry. *J. Chem. Phys.*, 96:517, 1992.

[36] H. Goldstein. *Classical Mechanics.* Addison-Wesley, 1980.

[37] D. M. Heyes. *J. Chem. Phys.*, 79:4010, 1983.

[38] M. J. L. Sangster and M. Dixon. *Adv. Phys.*, 25:247, 1976.

[39] L. Verlet. *Phys. Rev.*, 159:98, 1967.

[40] W. C. Swope, H. C. Andersen, P. H. Berens, and K. R. Wilson. *J. Chem. Phys.*, 76:637, 1982.

[41] J. P. Rose and R. S. Berry. *J. Chem. Phys.*, 98:3246, 1993.